International Journal of Earth Sciences (2020) 109:2081–2112
https://doi.org/10.1007/s00531-020-01889-7

ORIGINAL PAPER

Seawater-dominated, tectonically controlled and volcanic related geothermal systems: the case of the geothermal area in the northwest of the island of Euboea (Evia), Greece

Christos Kanellopoulos[1,2,3] · Markos Xenakis[3] · Panagiotis Vakalopoulos[3] · Haralambos Kranis[1] · Maria Christopoulou[4] · George Vougioukalakis[3]

Received: 4 January 2020 / Accepted: 30 May 2020 / Published online: 8 June 2020

Abstract
The northwest of the island of Euboea is located in a back-arc geological position, at the western extremity of the North Anatolian Fault. In that area, several hot springs occur in three locations (Ilia, Gialtra, Aedipsos; including newly found offshore-springs) with temperatures up to 84 °C, depositing ore-grade thermogenic travertine. The geothermal system is seawater-dominated and under pressure, using the local fault systems and is related to the Plio-Pleistocene Lichades volcanic centre. The whole area could be characterized as the lateral tips of a major fault segment, with the presence of complex networks of additional fault systems leading to fault intersections. That conclusion is also supported by the travitonic data. The geothermal fluids are near neutral pH, sodium-chloride and their chemistry is controlled by: (i) high seawater participation, (ii) a deep magmatic source and (iii) chemical composition of the bedrocks. Based on all the available data, including drilling and temperature logging data, the bedrock hosting the upflow circulation of the geothermal fluid is not in hydraulic connection with cold aquifers or permeable geological formations of the area. The local metamorphic rock formations are impermeable and work as a geothermal cap. Also, Aedipsos' vast deposit of thermogenic travertine probably acts as a second geothermal cap formation. However, at the same time, it presents serious thermal anomalies, since major geothermal fluid circulation has been identified inside its fractures. According to chemical geothermometers, the temperature of the geothermal reservoir is 140–164 °C. The typical geothermal gradients in the area are from 7.8 °C/100 m to 18.7 °C/100 m. In one case, an anomalous high geothermal gradient (53.9 °C/100 m) was found, most probably due to spatial shape diversity of the geothermal reservoir, a suggestion also supported by the estimated circulation depth of the geothermal fluid, which varies from area to area (~ 300–1800 m) and the fluid residence time (by ^{226}Ra–^{222}Rn method), which is around 80–100 years.

Keywords Geothermal energy · Tectonically controlled geothermal system · Seawater dominated geothermal system · Volcanic related geothermal system · Aedipsos (Edipsos or Aidipsos) · NW Euboea (Evia)

✉ Christos Kanellopoulos
ckanellopoulos@gmail.com

Markos Xenakis
markxen@igme.gr

Panagiotis Vakalopoulos
vakalo@igme.gr

Haralambos Kranis
hkranis@geol.uoa.gr

Maria Christopoulou
christopouloumaria@gmail.com

George Vougioukalakis
gvoug@igme.gr

[1] Department of Geology, University of Patras, 26500 Patras, Greece

[2] Department of Geology and Geoenvironment, National and Kapodistrian University of Athens, Panepistimioupolis, Ano Ilissia, 15784 Athens, Greece

[3] Hellenic Survey of Geology and Mineral Exploration (H.S.G.M.E.), 1st Spirou Louis St., Olympic Village, 13677 Acharnae, Greece

[4] Geologist, Sapfous 53, Kallithea, 17676 Athens, Greece

Introduction

The occurrence of a large number of hot springs in Greece is attributed to its geotectonic setting, which is mainly related to the convergence-subduction of African–European tectonic plates and the prolongation of the North Anatolian Fault into the Northern Aegean Sea. The resulting magmatic and volcanic processes, alongside the tectonic settings, favour the rise of deep gases that reach the surface to form fumaroles (e.g. Tassi et al. 2013a, b), and fluids that discharge at the ground surface or the seafloor, i.e. hot springs (e.g. Gkioni-Stavropoulou 1983; Orfanos 1985; Sfetsos 1988; Lambrakis and Kallergis 2005; Valsami-Jones et al. 2005; Price et al. 2013; Kilias et al. 2013; Kanellopoulos et al. 2017a, b).

In the northwest Euboea (Evia) island, several hot springs occur (in three areas: Aedipsos, Ilia, Gialtra). The Aedipsos hot springs have been known for their healing properties since antiquity. Even now, Aedipsos is one of the main thermal treatment and balneotherapy destinations in Greece (e.g. Charitakis 1935; Papanikolaou 1939; Kouskoukis 2014). According to ancient Greek mythology, the Aedipsos hot springs were created by the god Hephaestus, on request of the goddess Athena, so that the mythical hero Hercules could bath and recover his strength after his mythical labours. The great philosopher Aristotle in his study (Meteorology, II, 8.3, 340 B.C.) was the first who attempted to explain the operating principle of the Aedipsos hot springs. He suggested that the channelized seawater flowing beneath the island raised the pressure in the bedrock, thus causing earthquakes. As a result of friction, rock heated up as well the fluid, which discharged at the surface as hot springs.

Additionally, many ancient historians and modern scientists have made observations about the effect of strong historical earthquakes on the occurrence of Northern Euboeas' hot springs. During the historical earthquake of 426 B.C., which is mentioned by Thucydides in the "History of the Peloponnesian War" (chap. 3.89) and by Strabo in the "Geography" (Chap. 1.3.2), the hot springs of Aedipsos dried up. Still, after 3 days, new hot springs appeared in new positions. A part of the Lichades volcanic islands was submerged because of that earthquake. Also, during the Atalanti historical earthquake in 1894, the hot spring at Gialtra became turbid (Pertessis 1937) and new springs appeared in the area of Aedipsos (Margomenou-Leonidopoulou 1976). The earthquake did not cause any seismic sea wave (Ambraseys 2009).

The hot springs in Northern Euboea were among the first ones to be studied after the formation of the modern Greek State; research interest has been continued until today (Landerer 1836; Damvergis 1899; Gkioni-Stavropoulou 1983, 1998; Geotermica Italiana 1984; Shimizu et al. 2005; Hatzis et al. 2008; Kanellopoulos 2006, 2011, 2012, 2013; Kelepertsis et al. 2009; D'Alessandro et al. 2014; Dotsika 2015; Kanellopoulos et al. 2017a, b, 2018a). Euboeas' hot springs are of high importance not only for the potential geothermal heat capacity, but additionally because they are presenting active ore-mineralizing processes (Kanellopoulos et al. 2017a, 2018b, 2019a) and travertine deposition in terrestrial seawater-dominated hot springs environment (Kanellopoulos et al. 2017a, 2019a). Even though, several questions remain unanswered, such as the relation between the tectonic setting and the hot springs, information concerning the deep-water circulation pathways, the circulation depths and residence time and a synthetic assessment of all three areas of geothermal interest, i.e. Aedipsos, Ilia and Gialtra. Additionally, although data from drilling conducted in the area are available, yet no summarizing study exists, taking into consideration and synthesizing all the available information, including a re-evaluation of the geothermal gradients, an estimation of the potential geothermal heat capacity and a suggestion of a conceptual model.

Based on the hydrochemical and radiological analysis, re-evaluation and synthesis of all the available drilling and temperature logging data and a tectonic assessment, the aim of this paper is the investigation of the whole geothermal system of the northwestern part of Euboea, with an emphasis on: (i) the geochemical and the radiological content of the fluids and comparison with other geothermal areas, (ii) establishing the contribution of the local geology and especially the tectonic settings and the magmatic processes, to the studied geothermal system and (iii) assessment of the deep circulation parameters, such as circulation depth, residence time, calculation of the geothermal gradients, geothermal reservoir temperature and finally proposing a conceptual model.

Geological and structural setting of the study area

The study area is located at the western extremity of the North Anatolian Fault and near the Plio-Pleistocene volcanic centre of Lichades (Fig. 1). In the greater area, several hot springs occur, i.e. in the northwestern part of Euboea Island (hot spring sites: Aedipsos, Ilia and Gialtra, Fig. 1b) and the neighbouring eastern central part of the Greek mainland, namely the Sperchios Basin (hot spring sites: Kamena Vourla, Thermopylae, Ypati and Platistomo, Fig. 1b).

Northwest Euboea belongs to the Pelagonian and Sub-Pelagonian geotectonic units of the Hellenides (Aubouin 1959; Mountrakis 1986; Jolivet et al. 2013). In the studied area, a Permian–Triassic volcanoclastic complex overlies a

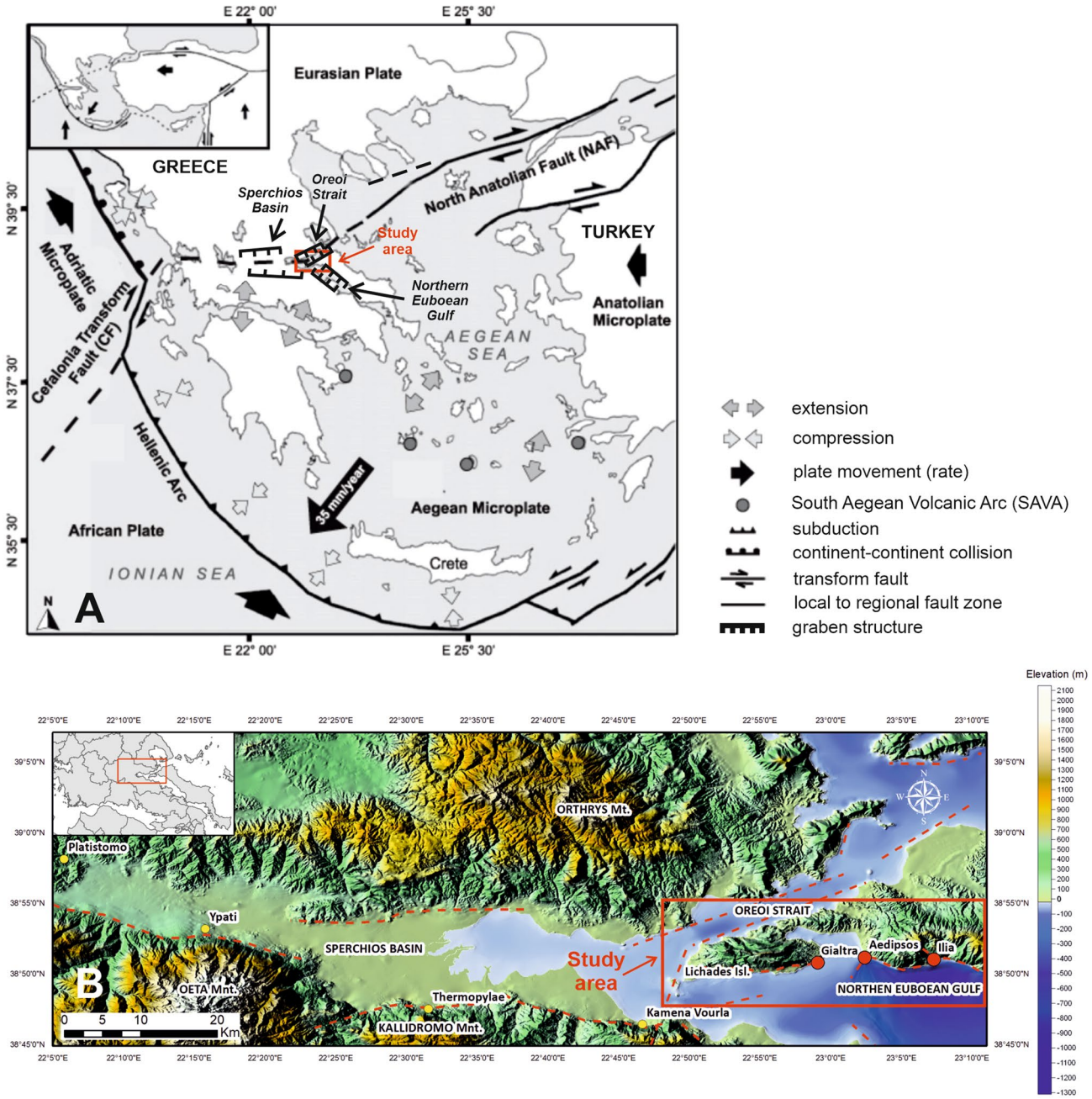

Fig. 1 **a** Plate boundaries and geodynamic pattern of the Aegean Sea plate, with emphasis on the Northern Euboean Gulf, the Oreoi Strait and Sperchios Basin areas (modified after Vött 2007; Ring et al. 2010). **b** Digital Elevation Model map [DEM, based on the official Greek topographical maps 1:50,000 for the land and the IGME (1991) and EMODnet bathymetric data for the sea] at a 25-m resolution of Northern Euboea island, Oreoi Strait, Northern Euboean Gulf and Eastern Central Greece (Sperchios Basin). The major neotectonic fault systems are symbolized with red dashed lines (based on the available data; IGME 1957, 1984, 1991; Galanakis 1997; Kranis 1999; Vavassis 2001) and the locations of the hot springs are symbolized with: red dots for NW Euboea area (studied sites), and yellow dots for Sperchios area. The geographical coordinates are in EGSA '87

pre-middle to middle Carboniferous metamorphic basement. It is overlain by middle Triassic shallow marine clastic and carbonate rocks intercalated with volcanic rocks. On top of this sequence, Jurassic limestones and Late Jurassic- Early Cretaceous ophiolites occur (Katsikatsos et al. 1982; IGME 1984; Scherreiks 2000; Figs. 2 and 3). In Northern Euboea, lignite layers formed inside Neogene-Lower Pleistocene lake sediments (Vakalopoulos et al. 2000).

Several hot springs discharge in Aedipsos, Ilia and Gialtra (Figs. 1b and 2), often accompanied by thermogenic

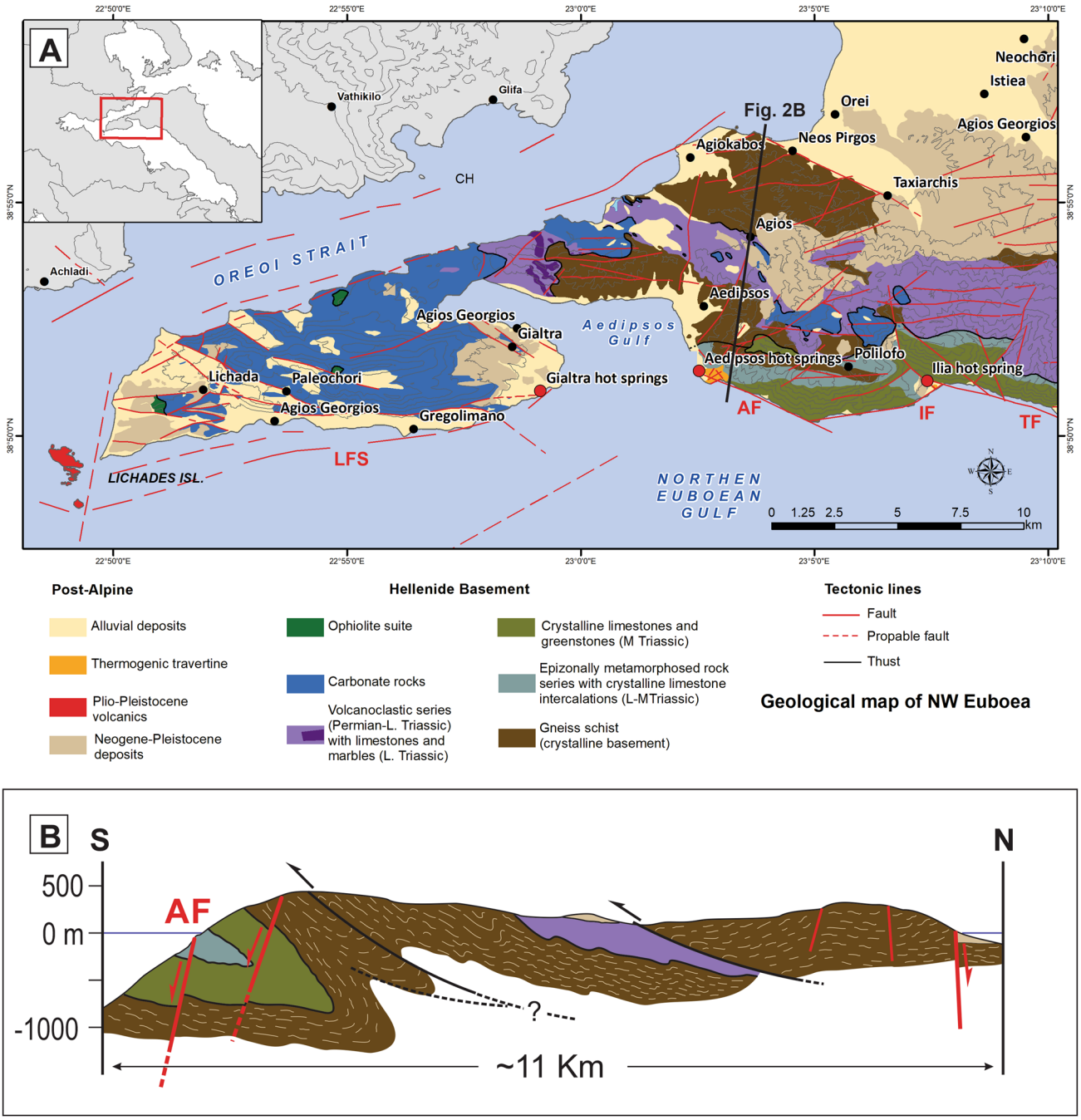

Fig. 2 **a** Geological map of the NW of Euboea [based on the published geological maps (IGME 1957, 1984) and other studies (IGME 1991; Galanakis 1997; Vakalopoulos et al. 2000; Vavassis 2001; Hatzis et al. 2008) and field observations]; *TF* = Telethrio Fault, *IF* = Ilia Fault, *AF* = Aedipsos Fault and *LFS* = Lichades Fault System. The red dots are the locations of the study sites. The geographical coordinates are in EGSA '87. **b** Geological cross-section across the study area, to show the structural and stratigraphical relationships among the mapped geological units

travertine deposits (Kanellopoulos 2011, 2012, 2013, 2014). Aedipsos is one of the largest active thermogenic travertine systems of Greece, producing a large variety of lithotypes and morphological types (Kanellopoulos 2012, 2013), since it covers an area of about 0.5 km^2, with a visible thickness of several meters. A large part of the city of Aedipsos is built on this travertine (Fig. 3).

The Northern Euboean Gulf is a part of a three graben-system: (i) to the west, the Sperchios graben is controlled by E–W to ESE–WNW range-bounding neotectonic normal

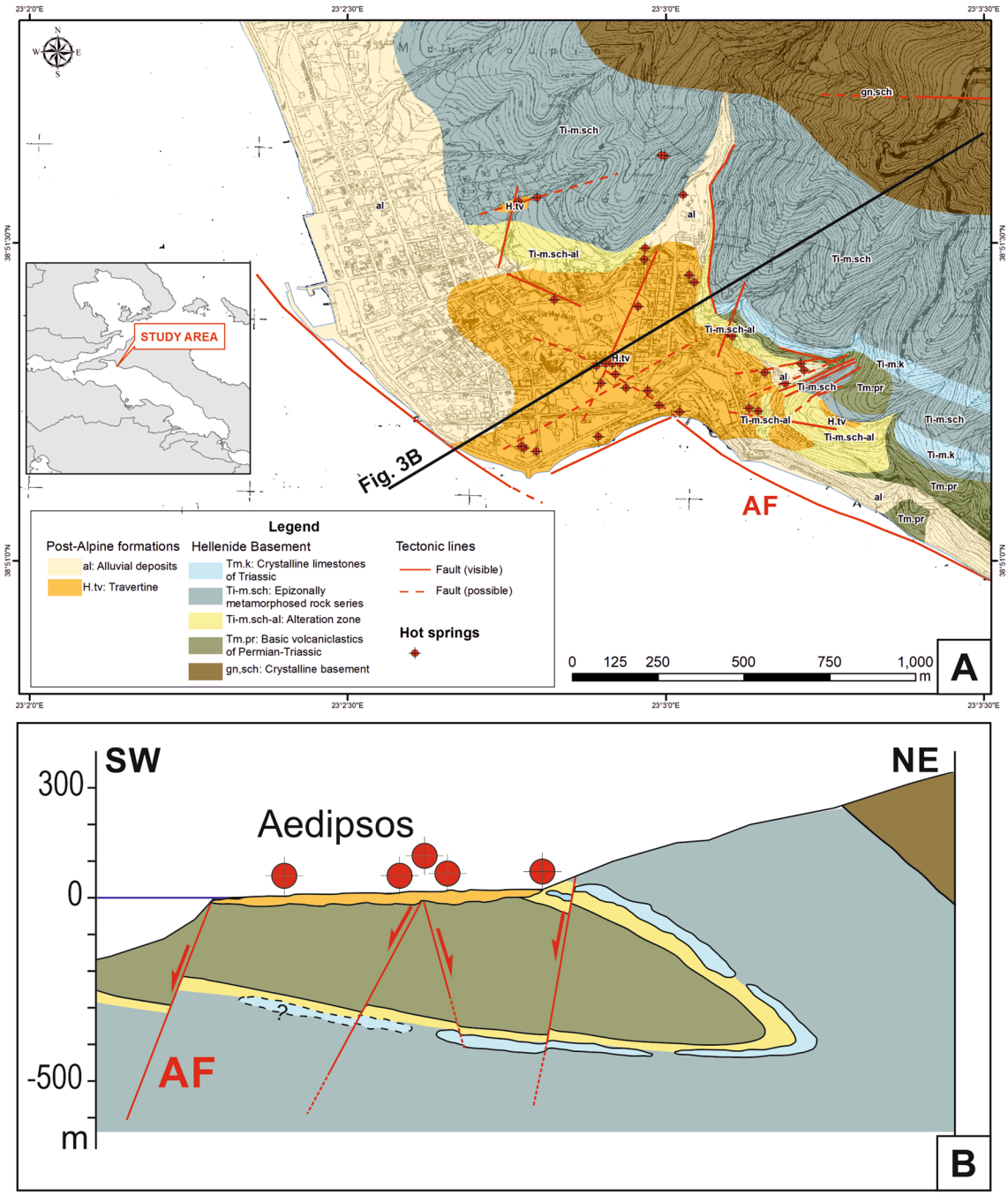

Fig. 3 **a** Geological map of the Aedipsos area [based on the published geological map (IGME 1984) and other studies (Tzitziras and Ilias 1996; Vavassis 2001) and field observations]; *AF* = Aedipsos Fault. All sampling sites are presented here, except for the Ilia and Gialtra samples, which are located in the relevant sites in Fig. 2. The geographical coordinates are in EGSA '87. **b** Geological cross-section across the Aedipsos area, showing the structural and stratigraphical relationships among the mapped geological units

faults; (ii) to the northeast, Oreoi Strait represents a narrow symmetrical NE–SW graben, with NE–SW striking neotectonics marginal faults, which occurs offshore as well as, on land (IGME 1991); and (iii) to the southeast, the Northern Euboean Gulf is ca. 100 km-long, NW–SE trending graben, bordered by large neotectonics normal fault zones of SE–NW to E–W direction (Roberts and Jackson 1991; Kranis 1999; Palyvos 2001; Pantosti et al. 2001; Fig. 1). The study area is located at the junction between the Euboea-Sperchios rift and the NE–SW Oreoi Strait. The initiation and evolution of these morphotectonic structures are possibly related to the propagation of the North Anatolian Fault

in the Aegean domain (e.g. McKenzie 1970, 1972; Shaw and Jackson 2010).

At the centre of the Northern Euboea Gulf, the Plio-Pleistocene volcanic centre of the Lichades occurs (Georgalas 1938, 1940; Gidarikos 1938; Pe-Piper and Piper 2002; Kanellopoulos et al. 2019b, Figs. 1b, 2), made up of 0.5 Ma-old trachyandesitic lava flows (whole-rock K–Ar method, Fytikas et al. 1976). Trachyandesitic lavas at the nearby Kamena Vourla were dated at 1.7 Ma (K–Ar method, Bellon et al. 1979). Magma emplacement took place along the major tectonic structures in the area (Kranis 1999). Many different theories were proposed about the geological setting of the Lichades volcanic complex. Ninkovich and Hays (1972), Pe (1975) and Pe and Panagos (1976) suggested that the Lichades volcanic centre could be the western continuation of the South Aegean active volcanic arc. Pe-Piper and Piper (1989) suggested that the Lichades volcanic centre together with trachytes and sodic basalts elsewhere in the Aegean could be related to the "aseismic subducted slab" at greater depths, than the arc volcanoes. Fytikas et al. (1985) and Pe-Piper and Piper (2007) proposed a possible genetic relation with the North Anatolia fault continuation. Innocenti et al. (2010) based on Sr–Nd–Pb isotopic data, related this volcanic centre to the vast volcanic belt that developed north of the Pelagonian–Attic–Cycladic-Menderes massifs, encompassing a 35 Ma timespan which is widespread over a large area from NW Greece–Macedonia to the Aegean-western Anatolia. Accordingly, the Euboea-Kamena Vourla volcanic products are orogenic in character and partially contemporaneous with the south Aegean active volcanic arc, but with different geochemical features, related to distinct magma sources (e.g. lithospheric mantle wedge and a depleted asthenospheric mantle wedge north and south of the Pelagonian–Attic–Cycladic–Menderes massifs, respectively).

Karastathis et al. (2011) showed that there is a magma chamber under the North Euboean Gulf area estimated at about 7–8 km depth, by combining a three-dimensional travel time inversion of microseismic data recorded by an on/offshore local seismic network and a Curie Point Depth analysis based on aeromagnetic data.

Materials and methods

Northern Euboea is a tectonically active area, with the neotectonic features, magmatic processes are present, and several hot springs occur. In such cases, the understanding and the exploration of geothermal systems is challenging, and various exploration methods need to be applied to achieve an in-depth understanding of the system (Cumming 2009). In every geothermal system, the first step in exploration is the geochemical study of the hot springs (Hochstein 1988). Afterwards, especially in active tectonic areas, where it is possible to have structural control of geothermal fluid flow, it has proven necessary to assess the role of fault zones and fractures (Goyal and Kassoy 1980; Banks et al. 1996; Caine et al. 1996; Marques et al. 2011). Faults are the preferred fluid pathways, where the pressure and temperature of the field are significantly different (Cherubini et al. 2013). Thus, such structures play a significant part in the recharge or discharge of the reservoir, as is shown in several studies of geothermal areas, e.g. Kakkonda (McGuinness et al. 1995) and Seferihisar–Balçova (Magri et al. 2010).

Hot water sampling and analysis

A total of 32 hot water samples were collected (Table 1) from hot springs, boreholes and surface streams used mainly for thermal spa/bathing therapies. Unstable parameters including pH, temperature and electrical conductivity (E.C.) were measured in the field, using portable apparatus.

Four sampling sites were selected as control points. From these four sites, samples were collected and analysed during both field trips (Artemis: STR-113GA-01 and -AD-13; Ilia: STR-117G18-01 and -IL-2; Ilios: STR-114P4-01 and -AD-1; Ntamaria: STR-113-01 and -AD-10) to evaluate possible hydrochemical changes over the period between the two visits.

During fieldwork, all the major hot springs of the area were spotted and located with handheld GPS, and several photos were taken in areas of interest using a thermal camera (FLIR T640).

For the chemical analysis, two vacuum-filtered, through 0.45 µm-pore size membrane filters aliquot of 1000 ml and 250 ml were collected, the second of which was acidified until 2% of nitric acid. Both were stored in a polyethylene container and preserved in a refrigerator.

Radiological analyses of ^{222}Rn and ^{226}Ra were conducted on selected samples by using a SARAD RTM 1688-2 portable device. The ^{222}Rn was measured in the field.

All 32 water samples were analysed in the Laboratories of Greek Geological Survey. Alkalinity (as HCO_3^-) was measured according to ISO 9963-1:1996 protocol. The major elements and ion concentrations were measured using spectrophotometer, titration and Inductively Coupled Plasma-Optical Emission Spectrometry (ICP-OES, Table 2). Trace elements concentrations were measured using Inductively Coupled Plasma-Mass Spectrometry (ICP-MS, Table 3).

Travertine samples and analysis

Representative samples from Aedipsos' travertines were collected. Even though travertine deposit was identified in Ilia

Table 1 Samples locality and use, physiochemical parameters and hydrochemical type

Station	Sample	Lon.[c]	Lat.[c]	Location	Locality	Date	Temp. (°C)	pH	E.C. (mS/cm)	T.D.S.[a] (mg/L)	Hydroc. type	Sampling site
STR-113	STR-113-AD-10	417283.20	4300846.70	Aedipsos	EOT-Ntamaria	25-09-2015	71.2	5.97	47850	32440	Na–Cl	Artesian borehole
STR-113	STR-113-AD-11	417,283.20	4,300,846.70	Aedipsos	EOT-Ntamaria	25-09-2015	65.6	6.76	48,180	33,380	Na–Cl	Drainage channel
STR-112A	STR-112A-GIA-1	411873.00	4300336.00	Gialtra	Gialta	24-09-2015	42.1	6.64	49770	35270	Na–Cl	Drainage channel
STR-113GA	STR-113GA-AD-13	417328.60	4300776.50	Aedipsos	EOT-Artemis	25-09-2015	78.8	5.97	49300	34970	Na–Cl	Artesian borehole
STR-113GA	STR-113GA-AD-12	417328.60	4300776.50	Aedipsos	EOT-Artemis	25-09-2015	65.1	6.92	50310	34820	Na–Cl	Drainage channel
STR-113GA	STR-113GA-EOT-3	417328.60	4300776.50	Aedipsos	EOT-Artemis-Wall	24-09-2015	80.8	6.12	49250	34265	Na–Cl	Artesian borehole
STR-113GA	STR-113GA-AD-14	417328.60	4300776.50	Aedipsos	EOT-Artemis	25-09-2015	51.3	6.25	18850	12550	Na–Cl	Artesian borehole
STR-117G18	STR-117G18-IL-2	424273.00	4300440.00	Ilia	Ilia	24-09-2015	63.5	5.88	34150	23160	Na–Cl	Artesian borehole
STR-114P4	STR-114P4-AD-1	417727.00	4300842.00	Aedipsos	Skourtanioti-Ilios	24-09-2015	57.3	6.63	40250	27140	Na–Cl	Spring
STR-114P4	STR-114P4-AD-2	417727.00	4300842.00	Aedipsos	Skourtanioti-Ilios	24-09-2015	48.9	7.39	40880	27790	Na–Cl	Drainage channel
STR-114P8	STR-114P8-RK-1	417476.00	4301103.00	Aedipsos	Pizou-Kapelari-Cave	25-09-2015	49.2	6.05	41690	28840	Na–Cl	Spring
STR-114P8	STR-114P8-RK-2	417476.00	4301103.00	Aedipsos	Pizou-Kapelari	25-09-2015	43.1	6.50	45710	30780	Na–Cl	Drainage channel
STR-114P8	STR-114P8-RK-3	417476.00	4301103.00	Aedipsos	Pizou-Kapelari	25-09-2015	37.2	6.27	48110	33950	Na–Cl	Drainage channel
STR-113G4	STR-113G4-EOT-2	417298.00	4300847.00	Aedipsos	EOT-G4	25-09-2015	61.9	6.00	42530	29660	Na–Cl	Artesian borehole
STR-113G4	STR-113G4-EOT-1	417298.00	4300847.00	Aedipsos	EOT-G4	25-09-2015	54.2	6.55	46590	32610	Na–Cl	Artesian borehole
STR-114P17	STR-114P17-KAS-1	417403.00	4300725.00	Aedipsos	City Hall	24-09-2015	52.4	7.16	44120	30020	Na–Cl	Drainage channel
STR-114P17	STR-114P17-KAS-2	417403.00	4300725.00	Aedipsos	City Hall	24-09-2015	40.1	7.26	43130	29170	Na–Cl	Drainage channel
STR-114P17	STR-114P17-KAS-3	417403.00	4300725.00	Aedipsos	City Hall-Wall	24-09-2015	55.8	6.34	28390	18590	Na–Cl	Spring
STR-113	STR-113-01	417283.20	4300846.70	Aedipsos	EOT-Ntamaria	20-05-2015	70.1	6.04	48630	32530	Na–Cl	Artesian borehole
STR-115G7	STR-115G7-01	417644.10	4300818.03	Aedipsos	Kompogianni	20-05-2015	71.9	6.21	48190	33365	Na–Cl	Artesian borehole
STR-112A	STR-112A-01	411,873.00	4,300,336.00	Gialtra	Gialta	21-05-2015	43.4	6.50	50,230	34,685	Na–Cl	Spring
STR-113GA	STR-113GA-01	417,328.60	4,300,776.50	Aedipsos	EOT-Artemis	20-05-2015	79.6	6.16	49,580	33,575	Na–Cl	Artesian borehole
STR-117G18	STR-117G18-01	424,273.00	4300440.00	Ilia	Ilia	19-05-2015	63.7	6.07	34,410	22,690	Ca–Na-Cl	Artesian borehole
STR-114P2	STR-114P2-2	417,607.00	4,300,714.00	Aedipsos	Skourtanioti-Frini	20-05-2015	64.3	6.25	45,910	30,875	Na–Cl	Spring
STR-114P4	STR-114P4-01	417,727.00	4,300,842.00	Aedipsos	Skourtanioti-Ilios	20-05-2015	58.1	6.83	41,330	27,350	Na–Cl	Spring
STR-114P5	STR-114P5-01	417,561.00	4,300,935.00	Aedipsos	Ai pigai	20-05-2015	54.5	6.60	45,220	30,585	Na–Cl	Spring
STR-114P8	STR-114P8-01	417,476.00	4,301,103.00	Aedipsos	Pizou-Kapelari-Wall	20-05-2015	60.2	6.04	48,260	32,195	Na–Cl	Spring
STR-114P9	STR-114P9-01	417,374.00	4,301,149.00	Aedipsos	Papaioannou	21-05-2015	43.9	6.40	29,900	18,800	Na–Cl	Artesian borehole
STR-114P1A	STR-114P1A-01	417,376.00	4,301,182.00	Aedipsos	Thermopotamos	20-05-2015	69	6.21	41,500	27,400	Na–Cl	Spring
STR-114G20	STR-114G20-01	417,090.00	4,301,320.00	Aedipsos	Koukoumos	20-05-2015	82.2	6.50	49,680	33,735	Na–Cl	Artesian borehole
STR-BR1	STR-BR1-1	417,628.10	4,300,705.26	Aedipsos	Vrysakia	21-05-2015	54	6.56	32,700	20,870	Na–Cl	Spring
STR-116G3	STR-116G3-1	417,122.12	4,300,592.96	Aedipsos	Thermae Sylla	20-05-2015	48.7	6.47	47,470	32,330	Na–Cl	Borehole
SW[a]	SW[a]	–	–	Aegean Sea	Aegean Sea	–	25.9	8.18	56,350	40,900	Na–Cl	Aegean sea

Geographical coordinates are in EGSA '87

[a]Seawater analyses from Aegean Sea (Athanasoulis et al. 2016)

[b]Measured at the laboratory

Table 2 Concentrations of major ions (in mg/L) and ion ratios

Sample	Ca^{2+}	Mg^{2+}	Na^{+}	K^{+}	HCO_3^{-}	Cl^{-}	SO_4^{2-}	NO_3^{-}	NH_4^{+}	NO_2^{-}	F^{-}	SiO_2^{-}	Li/B	Cl/Br	Cl/B	K/Cl	Na/Cl	Ca/Cl	Li/Cl	HCO_3/Cl	Mg/Cl	Ca/Na	Cl/SO_4
STR-113-AD-10	1416	254	10706	308	612	18298	536	< 5	0.4	< 0.05	4.7	47.3	0.14	387	2158	0.017	0.585	0.077	0.000065	0.033	0.014	0.132	34.14
STR-113-AD-11	1371	255	11054	316	545	18438	1121	< 5	0.55	< 0.05	4.6	47.5	0.14	388	2149	0.017	0.600	0.074	0.000067	0.030	0.014	0.124	16.45
STR-112A-GIA-1	1460	480	11029	304	264	19150	2441	< 5	0.11	0.14	2.5	24.4	0.10	391	4517	0.016	0.576	0.076	0.000022	0.014	0.025	0.132	7.85
STR-113GA-AD-13	1402	270	11641	329	602	19290	1122	5.6	0.37	< 0.05	4.8	48.6	0.15	453	2167	0.017	0.603	0.073	0.000070	0.031	0.014	0.120	17.19
STR-113GA-AD-12	1404	273	11523	337	459	19430	1161	< 5	0.55	< 0.05	4.5	48.2	0.15	456	2135	0.017	0.593	0.072	0.000069	0.024	0.014	0.122	16.74
STR-113GA-EOT-3	1353	268	11610	325	593	19290	1122	< 5	0.6	< 0.05	4.7	47.9	0.13	427	2172	0.017	0.602	0.070	0.000059	0.031	0.014	0.117	17.19
STR-113GA-AD-14	642	140	3870	110	661	6345	444	< 5	0.76	0.58	3.5	32.4	0.12	599	1866	0.017	0.610	0.101	0.000066	0.104	0.022	0.166	14.29
STR-117G18-IL-2	1417	186	6943	181	637	12553	811	< 5	1.93	< 0.05	3.6	102.0	0.20	312	1291	0.014	0.553	0.113	0.000151	0.051	0.015	0.204	15.48
STR-114P4-AD-1	1148	201	8690	260	515	15177	881	< 5	0.52	0.28	4.2	40.1	0.10	422	2120	0.017	0.573	0.076	0.000048	0.034	0.013	0.132	17.23
STR-114P4-AD-2	1120	207	9001	271	340	15745	929	< 5	0.42	0.29	4.1	40.9	0.10	463	2139	0.017	0.572	0.071	0.000046	0.022	0.013	0.124	16.95
STR-114P8-RK-1	1149	228	9418	272	614	15885	961	< 5	0.4	< 0.05	4.6	46.4	0.18	416	2482	0.017	0.593	0.072	0.000071	0.039	0.014	0.122	16.53
STR-114P8-RK-2	1144	229	9637	267	609	17589	989	< 5	0.49	< 0.05	4.6	46.1	0.15	305	2314	0.015	0.548	0.065	0.000064	0.035	0.013	0.119	17.78
STR-114P8-RK-3	1318	264	11155	313	626	18866	1090	< 5	0.38	< 0.05	4.6	46.6	0.15	415	2144	0.017	0.591	0.070	0.000070	0.033	0.014	0.118	17.31
STR-113G4-EOT-2	1201	233	9638	274	680	16309	973	< 5	0.37	0.08	4.6	44.9	0.15	316	2146	0.017	0.591	0.074	0.000068	0.042	0.014	0.125	16.76
STR-113G4-EOT-1	1297	255	10835	304	567	18014	1048	< 5	0.81	0.12	4.5	46.1	0.15	308	2170	0.017	0.601	0.072	0.000068	0.031	0.014	0.120	17.19
STR-114P17-KAS-1	1269	224	9834	289	330	16877	983	< 5	0.99	0.5	4.2	45.2	0.12	355	2250	0.017	0.583	0.075	0.000051	0.020	0.013	0.129	17.17
STR-114P17-KAS-2	1210	222	9590	281	251	16453	991	< 5	0.77	< 0.05	4	42.0	0.11	388	2223	0.017	0.583	0.074	0.000050	0.015	0.013	0.126	16.60
STR-114P17-KAS-3	832	150	6002	178	400	10141	638	< 5	0.28	5.35	4.2	46.8	0.10	362	1988	0.018	0.592	0.082	0.000048	0.039	0.015	0.139	15.89
STR-113-01	1642	321	10219	351	620	18722	950	< 5	0.44	< 0.05	4.7	17.0	0.26	340	3546	0.019	0.546	0.088	0.000073	0.033	0.017	0.161	19.71
STR-115G7-01	675	313	10469	344	691	19006	1200	< 5	0.44	< 0.05	4.6	18.2	0.42	347	3801	0.018	0.551	0.036	0.000110	0.036	0.016	0.064	15.84
STR-112A-01	1641	621	10541	337	265	19006	2400	< 5	0.15	< 0.05	3	8.0	1.44	429	34746	0.018	0.555	0.086	0.000042	0.014	0.033	0.156	7.92
STR-113GA-01	1650	322	10500	361	585	19290	1150	< 5	0.5	< 0.05	4.8	16.4	0.25	348	3572	0.019	0.544	0.086	0.000071	0.030	0.017	0.157	16.77
STR-117G18-01	1571	233	6755	206	636	12765	800	< 5	0.57	< 0.05	3.8	47.0	0.37	335	1388	0.016	0.529	0.123	0.000263	0.050	0.018	0.233	15.96
STR-114P2-2	1584	301	9668	330	678	17589	1050	< 5	0.41	< 0.05	4.6	16.5	0.38	355	3490	0.019	0.550	0.090	0.000108	0.039	0.017	0.164	16.75
STR-114P4-01	1346	264	8546	294	568	15601	1000	< 5	0.44	< 0.05	4.4	17.6	0.36	355	3341	0.019	0.548	0.086	0.000109	0.036	0.017	0.158	15.60

Table 2 (continued)

Sample	Ca^{2+}	Mg^{2+}	Na^{+}	K^{+}	HCO_3^-	Cl^-	SO_4^{2-}	NO_3^-	NH_4^+	NO_2^-	F^-	SiO_2^-	Li/B	Cl/Br	Cl/B	K/Cl	Na/Cl	Ca/Cl	Li/Cl	HCO_3/Cl	Mg/Cl	Ca/Na	Cl/SO_4
STR-114P5-01	1496	288	9459	321	657	17730	950	< 5	0.43	< 0.05	4.3	16.2	0.28	374	3733	0.018	0.534	0.084	0.000074	0.037	0.016	0.158	18.66
STR-114P8-01	1620	313	9679	335	626	18722	1200	< 5	0.41	< 0.05	4.5	17.1	0.43	345	3821	0.018	0.517	0.087	0.000112	0.033	0.017	0.167	15.60
STR-114P9-01	864	174	5980	204	598	10567	700	< 5	0.37	< 0.05	3.7	17.7	0.23	323	2856	0.019	0.566	0.082	0.000081	0.057	0.016	0.144	15.10
STR-114P1A-01	1379	267	8551	293	593	15601	1000	< 5	0.65	< 0.05	4.1	16.4	0.43	331	3490	0.019	0.548	0.088	0.000122	0.038	0.017	0.161	15.60
STR-114G20-01	1668	322	10592	363	610	19574	900	< 5	0.56	< 0.05	4.6	16.2	0.27	365	3793	0.019	0.541	0.085	0.000072	0.031	0.016	0.157	21.75
STR-BR1-1	1079	220	6490	217	619	11843	700	< 5	0.31	< 0.05	3.4	16.3	0.26	335	3245	0.018	0.548	0.091	0.000079	0.052	0.019	0.166	16.92
STR-116G3-1	1357	484	10133	354	489	18298	1450	< 5	0.26	< 0.05	4.5	13.8	1.44	362	17765	0.019	0.554	0.074	0.000081	0.027	0.026	0.134	12.62
SW[a]	475	1160	13240	423	168	22270	3257	< 5	< 0.05	< 0.05	2.45	5	0.01	255	1614	0.019	0.595	0.021	0.000008	0.008	0.052	0.036	6.8

[a]Seawater analyses from Aegean Sea (Athanasoulis et al. 2016)

area, since the occurrence is limited, no sample was collected from that area.

The mineralogical compositions of the main mineral phases in travertines were identified mainly by optical microscopy and X-Ray Diffraction. XRD analysis was carried out using a Siemens Model 5005 X-ray diffractometer, Cu Ka radiation at 40 kV, 40 nA, 0.0200 step size and 1.0 s step time. The XRD patterns were evaluated using the EVA program of the Siemens DIFFRACplus and the D5005 software package.

The travertine samples were analysed for whole rock geochemistry after drying and pulverizing in an agate mortar and mill to < 0.075 mm. The samples were digested with HNO_3 and analysed by Inductively Coupled Plasma–Atomic Emission Spectroscopy method (ICP-AES) for Ca, Na, P, S, Si and by Inductively Coupled Plasma-Mass Spectrometry method (ICP-MS) for the trace elements.

Statistical analysis and use of GIS

Multivariate statistical analyses are valuable tools in environmental (e.g. Kanellopoulos and Argyraki 2013) and hydrochemical studies (e.g. Voudouris et al. 1997; Vega et al. 1998; Liu et al. 2003; Cloutier et al. 2008; Voutsis et al. 2015), since they can identify the factors that affect the chemical composition of the groundwater. Recently, multivariate statistical analyses were also applied to geothermal studies (e.g. Hernández-Antonio et al. 2015; Lindsey et al. 2018).

Factor analysis (Howarth and Govett 1983) was the main technique applied for statistical analysis, using samples only from hot springs and boreholes. This technique can simplify a complex data set by identifying one or more underlying 'factors' that might explain the dimensions associated with data variability. A varimax rotation was applied to the initial factor loadings to maximize the variance of the squared loadings. Additionally, clusters were created based on the correlation coefficient similarity of the parameters (Anderberg 1973).

A spatial database was developed in ArcGIS, including all the physicochemical parameters and elemental concentrations for each sampling point. Based on that, to visualize the spatial distribution of the shallow geothermal fluid circulation temperature in the Aedipsos area, the kriging interpolation method (Oliver 1990) was applied in the temperature measurements.

A new geological map of Aedipsos area (scale 1:10,000), was constructed, based on, the Greek Geological Survey published geological map (IGME 1984), other studies (Tzitziras and Ilias 1996; Vavassis 2001) and field observations. For the greater area of NW Euboea, a new geological map was also compiled, based on information from the Greek Geological Surveys' published geological maps

Table 3 Concentrations of trace elements (in µg/L)

Sample	Ag	Al	As	B	Ba	Be	Br	Cd	Co	Cr	Cu	Fe	Hg	I	Li	Mn	Mo	Ni	Pb	Rb	Sb	Se	Sr	U	V	Zn
STR-113-AD-10	< 5	< 10	120	8480	230	< 0.005	47300	< 1	< 10	< 10	130	1500	< 1	530	1190	53	< 10	85	< 5	170	< 5	440	11780	< 5	94	30
STR-113-AD-11	< 5	< 10	130	8580	230	< 0.005	47500	< 1	< 10	< 10	130	1260	< 1	560	1240	40	< 10	85	< 5	190	< 5	430	12000	< 5	110	< 10
STR-112A-GIA-1	< 5	< 50	160	4240	70	< 0.005	49000	< 1	< 10	< 10	120	345	< 1	560	420	< 10	< 10	90	< 5	108	< 5	490	9600	< 5	120	< 10
STR-113GA-AD-13	< 5	< 10	140	8900	270	< 0.005	42600	< 1	< 10	< 10	140	490	< 1	590	1350	27	< 10	93	< 5	195	< 5	470	12500	< 5	130	< 10
STR-113GA-AD-12	< 5	30	140	9100	260	< 0.005	42600	< 1	< 10	< 10	140	440	< 1	570	1350	20	< 10	90	< 5	200	< 5	480	12350	< 5	130	< 10
STR-113GA-EOT-3	< 5	< 10	130	8880	270	< 0.005	45200	< 1	< 10	< 10	140	510	< 1	550	1130	28	< 10	94	< 5	19	< 5	480	10700	< 5	150	< 10
STR-113GA-AD-14	< 5	20	72	3400	180	< 0.005	10600	< 1	< 10	< 10	50	6900	< 1	150	420	16	< 10	40	< 5	74	< 5	170	4750	< 5	62	< 10
STR-117G18-IL-2	< 5	< 50	250	9720	190	< 0.005	40260	< 1	< 10	< 10	72	11300	< 1	560	1900	380	< 10	75	< 5	220	< 5	310	18000	< 5	80	< 10
STR-114P4-AD-1	< 5	< 50	130	7160	170	< 0.005	36000	< 1	< 10	< 10	96	158	< 1	420	730	87	< 10	60	< 5	130	< 5	380	8000	< 5	110	< 10
STR-114P4-AD-2	< 5	< 50	120	7360	160	< 0.005	34000	< 1	< 10	< 10	90	137	< 1	430	730	45	< 10	56	< 5	140	< 5	280	7950	< 5	110	< 10
STR-114P8-RK-1	< 5	< 10	110	6400	150	< 0.005	38200	< 1	< 10	< 10	110	1900	< 1	380	1120	43	< 10	82	< 5	170	< 5	390	10700	< 5	140	< 10
STR-114P8-RK-2	< 5	60	110	7600	150	< 0.005	57700	< 1	< 10	< 10	110	1070	< 1	430	1120	43	< 10	82	< 5	170	< 5	400	10700	< 5	140	< 10
STR-114P8-RK-3	< 5	< 10	140	8800	230	< 0.005	45500	< 1	< 10	< 10	130	2580	< 1	450	1320	40	< 10	88	< 5	190	< 5	470	12500	< 5	150	< 10
STR-113G4-EOT-2	< 5	< 10	120	7600	250	< 0.005	51600	< 1	< 10	< 10	110	5000	< 1	400	1110	22	< 10	82	< 5	170	< 5	430	10800	< 5	130	< 10
STR-113G4-EOT-1	< 5	< 10	140	8300	250	< 0.005	58400	< 1	< 10	< 10	120	380	< 1	490	1230	17	< 10	86	< 5	180	< 5	460	11700	< 5	130	< 10
STR-114P17-KAS-1	< 5	< 50	100	7500	240	< 0.005	47600	< 1	< 10	< 10	110	32	< 1	480	865	< 10	< 10	85	< 5	180	< 5	400	9300	< 5	98	< 10
STR-114P17-KAS-2	< 5	< 50	100	7400	240	< 0.005	42400	< 1	< 10	< 10	120	29	< 1	490	820	< 10	< 10	80	< 5	150	< 5	400	8800	< 5	100	< 10
STR-114P17-KAS-3	< 5	< 50	62	5100	170	< 0.005	28000	< 1	< 10	< 10	62	10	< 1	280	490	55	< 10	55	< 5	100	< 5	270	570	< 5	70	< 10
STR-113-01	< 5	< 10	68	5280	240	< 0.005	55000	< 1	< 10	70	155	2500	< 0.5	415	1370	53	< 10	66	< 10	170	< 5	320	11300	< 5	73	< 50
STR-115G7-01	< 5	< 10	97	5000	220	< 0.005	54700	< 1	< 10	55	200	3170	< 0.5	415	2100	160	< 10	97	22	170	< 5	290	13230	< 5	110	< 50
STR-112A-01	< 5	< 10	82	547	70	< 0.005	44300	< 1	< 10	< 50	190	790	< 0.5	575	790	< 50	< 10	88	23	100	< 5	320	120	< 5	100	< 50
STR-113GA-01	< 5	< 10	68	5400	250	< 0.005	55500	< 5	< 10	< 50	150	540	< 0.5	430	1360	< 50	< 10	74	< 10	170	< 5	340	11300	< 5	70	< 50
STR-117G18-01	< 5	< 10	150	9200	210	< 0.005	38100	< 5	< 10	< 50	130	13300	< 0.5	500	3360	500	< 10	80	20	190	< 5	220	24000	< 5	70	< 50
STR-114P2-2	< 5	< 10	97	5040	200	< 0.005	49500	6	< 10	< 50	190	2400	< 0.5	550	1900	200	< 10	90	29	160	< 5	290	12750	< 5	100	< 50
STR-114P4-01	< 5	< 10	100	4670	200	< 0.005	44000	< 5	< 10	< 50	180	165	< 0.5	410	1700	180	< 10	80	20	150	< 5	260	11250	< 5	100	< 50
STR-114P5-01	< 5	< 10	64	4750	150	< 0.005	47400	< 5	< 10	< 50	140	2900	< 5	535	1320	140	< 10	69	< 10	170	< 5	300	10700	< 5	68	< 50
STR-114P8-01	< 5	< 10	100	4900	210	< 0.005	54300	7	< 10	< 50	205	1170	< 0.5	420	2100	< 50	< 10	100	25	170	< 5	290	13170	< 5	120	< 50
STR-114P9-01	< 5	< 10	60	3700	130	< 0.005	32700	< 5	< 10	< 50	100	880	< 0.5	300	860	210	< 10	< 50	< 10	107	< 5	200	640	< 5	50	< 50
STR-114P1A-01	< 5	100	780	4470	270	< 0.005	47100	< 5	< 10	< 50	170	520	< 0.5	425	1900	< 50	< 10	83	25	150	< 5	290	11220	< 5	110	< 50

Table 3 (continued)

Sample	Ag	Al	As	B	Ba	Be	Br	Cd	Co	Cr	Cu	Fe	Hg	I	Li	Mn	Mo	Ni	Pb	Rb	Sb	Se	Sr	U	V	Zn
STR-114G20-01	< 5	< 10	50	5160	130	< 0.005	53600	< 5	< 10	< 50	85	1020	< 0.5	445	1400	< 50	< 10	70	< 10	180	< 5	310	620	< 5	50	< 50
STR-BR1-1	< 5	< 10	50	3650	140	< 0.005	35400	< 5	< 10	< 50	100	870	< 0.5	325	940	160	< 10	53	< 10	130	< 5	210	790	< 5	50	< 50
STR-116G3-1	< 5	< 10	72	1030	130	< 0.005	50600	< 5	< 10	< 50	190	77	< 0.5	580	1480	270	< 10	70	34	150	< 5	290	11500	< 5	100	< 50
SW[a]	–	105	< 10	13800	< 10	–	87300	–	–	–	120	52	–	–	3360	< 10	30	–	–	–	–	–	5800	–	–	< 30

[a]Seawater analyses from Aegean Sea (Athanasoulis et al. 2016)

(IGME 1957, 1984), other studies (IGME 1991; Galanakis 1997; Vakalopoulos et al. 2000; Vavassis 2001; Hatzis et al. 2008) and field observations. Moreover, a 25-m resolution Digital Elevation Model (DEM) map of the area was created in this paper showing the major fault systems, using available topographical data and tectonic data of the area (IGME 1957, 1984, 1991; Galanakis 1997; Kranis 1999; Vavassis 2001; Fig. 2). All maps were compiled in ArcGIS, where the above-mentioned spatial database was developed.

Analytical results

Hot water chemical analysis

All sample locations are presented in Table 1 and Fig. 2 and 3; Tables 1, 2 and 3 show the physicochemical and chemical parameters analysed in situ and the laboratory.

Focusing on the samples from the hot springs and boreholes, the temperatures of the fluids varies from 43.4 to 82.2 °C. The highest temperatures were recorded in Aedipsos area (up to 82.2 °C). All samples are characterized as slightly acidic to near-neutral since the pH values vary from 5.88 to 6.83. The lowest pH value (5.88) was measured in Ilia hot spring and the highest values in the Aedipsos samples (up to 6.83). Total Dissolved Solids (T.D.S.) and Electrical Conductivity (E.C.) vary from 12.55 to 34.97 g/L and from 18.85 to 50.23 S/cm, respectively, with maximum values measured in Gialtra sample (TDS: 34.97 g/L and EC: 50.23 S/cm) and lower values in samples from Aedipsos area.

Classification of the studied fluid samples according to their major aqueous species content was assessed by plotting the major ion concentrations on a Piper diagram (Fig. 4a) revealing the very limited distribution of the studied samples and only Na–Cl water type, indicating a high degree of Na and Cl participation. The only exception is the STR-117G18-01 (Ilia area, rain season sample) with Ca–Na–Cl water type, which during the second sampling period STR-117G18-IL-2 (dry season sample), the water type was Na–Cl.

The Cl-SO_4-HCO_3 ternary diagram (Giggenbach 1981) was used to indicate the characteristics of the fluids (Fig. 4b). The studied geothermal fluids were classified as deep waters with volcanic origin affinities. Addictingly, in the Na–K–$\sqrt{Mg}$ diagram (Giggenbach 1988, Fig. 4c), all the samples are plotted in the same area and characterized as partially equilibrated waters. The Aedipsos fluids are plotted closer to the fully equilibrated line.

The comparison between samples collected during two periods (Artemis: STR-113GA-01 and -AD-13; Ilia: STR-117G18-01 and -IL-2; Ilios: STR-114P4-01 and -AD-1; Ntamaria: STR-113-01 and -AD-10) showed almost no

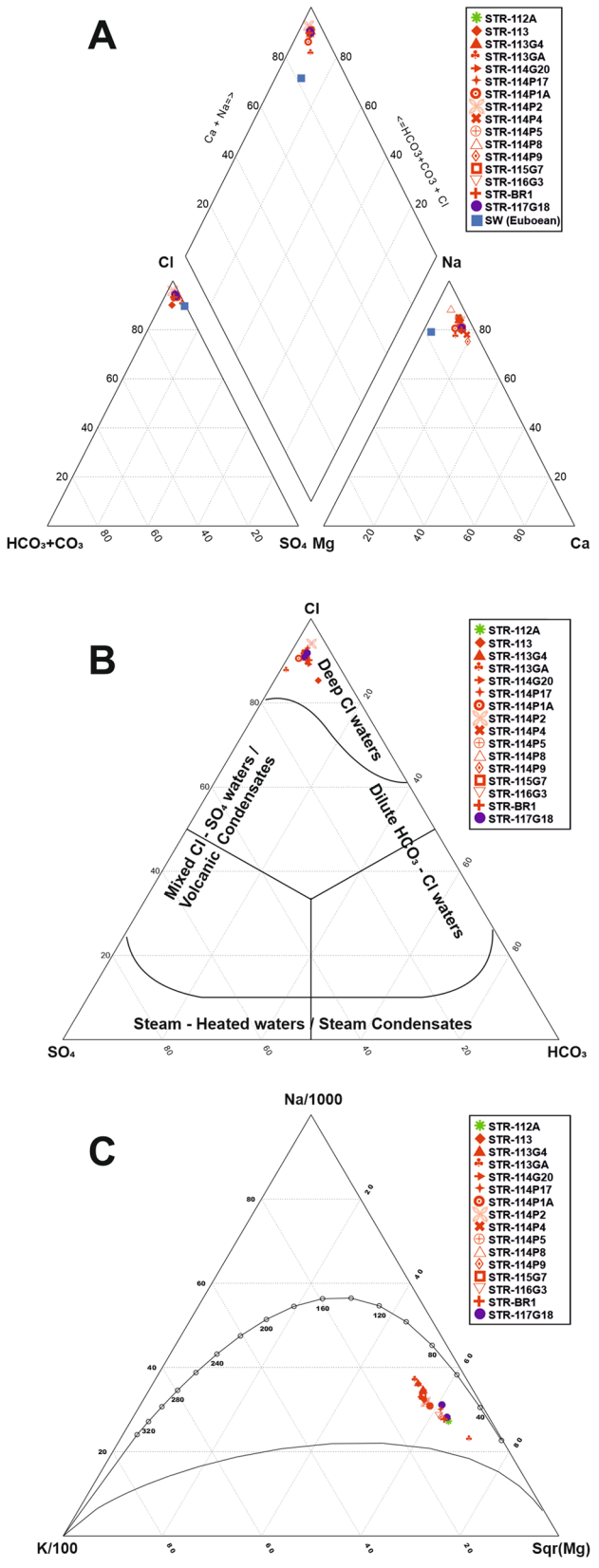

Fig. 4 Chemical composition of the studied geothermal fluid samples from only hot springs and boreholes plotted in **a** Piper diagram, **b** Cl–SO_4–HCO_3 ternary diagram (modified after Giggenbach,1988; Nicholson 1993) and **c** Na–K–Mg diagram (Giggenbach 1988)

difference in terms of pH, temperature, E.C. and limited variations in trace element concentrations (Tables 1, 2 and 3).

Chloride and sodium are the dominant anion (up to 1.96%) and cation (up to 1.16%), respectively. They show a very strong correlation ($R^2 = 0.95$, Fig. 5a), suggesting that they have a common origin, like seawater and/or a deep Na–Cl geothermal fluid member. The studied geothermal fluids also showed high concentrations in a series of ions and trace elements, which could be associated with seawater and/or likely to be of deep thermal origin. For example, conservative constituents (Tables 2, 3; Fig. 5b, c), such as F (up to 4.82 mg/L), B (up to 9.72 mg/L), SiO_2 (up to 102 mg/L), Br (up to 58.4 mg/L) and Li (up to 3.36 mg/L).

Moreover, the studied fluids showed high concentrations into some additional ions and trace elements, including metals (Fig. 5b, c), such as SO_4 (up to 2400 mg/L), Ca (up to 1668 mg/L), Sr (up to 24 mg/L), Fe (up to 13.3 mg/L), As (up to 0.78 mg/L) and Cu (up to 0.2 mg/L). These elements/ions ought to be related to the geological formations of the area, and some of them are associated with the travertine deposition.

On the Cl versus Br plot (Fig. 5d), the samples from hot springs and boreholes plot in a good linear correlation ($R^2 = 0.78$). In most samples the Cl/Br ratio (Table 2) is higher than that of seawater, suggesting that the high-salinity of these geothermal fluids is not only due to seawater participation in the deep part of the geothermal system.

However, Cl versus B (Fig. 5e) and Cl versus Li (Fig. 5f), which are also conservative constituents, are not in good correlation. High Cl/B ratio and high Cl concentrations, similar to the studied samples, are usually observed in the cases of mixing with seawater and/or some deep Na–Cl geothermal fluid member. The concentration of B and Li ranges from 0.55 to 9.7 mg/L and 0.42 to 3.36 mg/L, respectively. Almost all samples present excess B and Li compared to seawater, and in most cases, other ratios like K/Cl, Na/Cl, Ca/Cl and Li/Cl (Table 2) are higher or near the seawater value.

Hot water statistical analysis

The statistical summary of the analytical results of studied samples from hot springs and boreholes is presented in Table 4. With respect to median values (Fig. 5b, c), geothermal fluids are enriched in Cl (17,660 mg/L), Na (9653 mg/L), Ca (1368 mg/L), SO_4 (967 mg/L), Br (46.15 mg/L), Sr (11.23 mg/L), B (5.13 mg/L), Li (1.33 mg/L) and some samples in Fe (median 0.95 mg/L and max. value 13.3 mg/L) and As (median 0.1 mg/L and max. value 0.78 mg/L).

The correlation coefficients (Table 5) between elements related to seawater, i.e. Cl and Na, K, Mg, E.C. and TDS, are very high (> 0.8). Similarly, high correlation coefficients were identified between Cu and Ni, i.e. 0.7, suggesting some

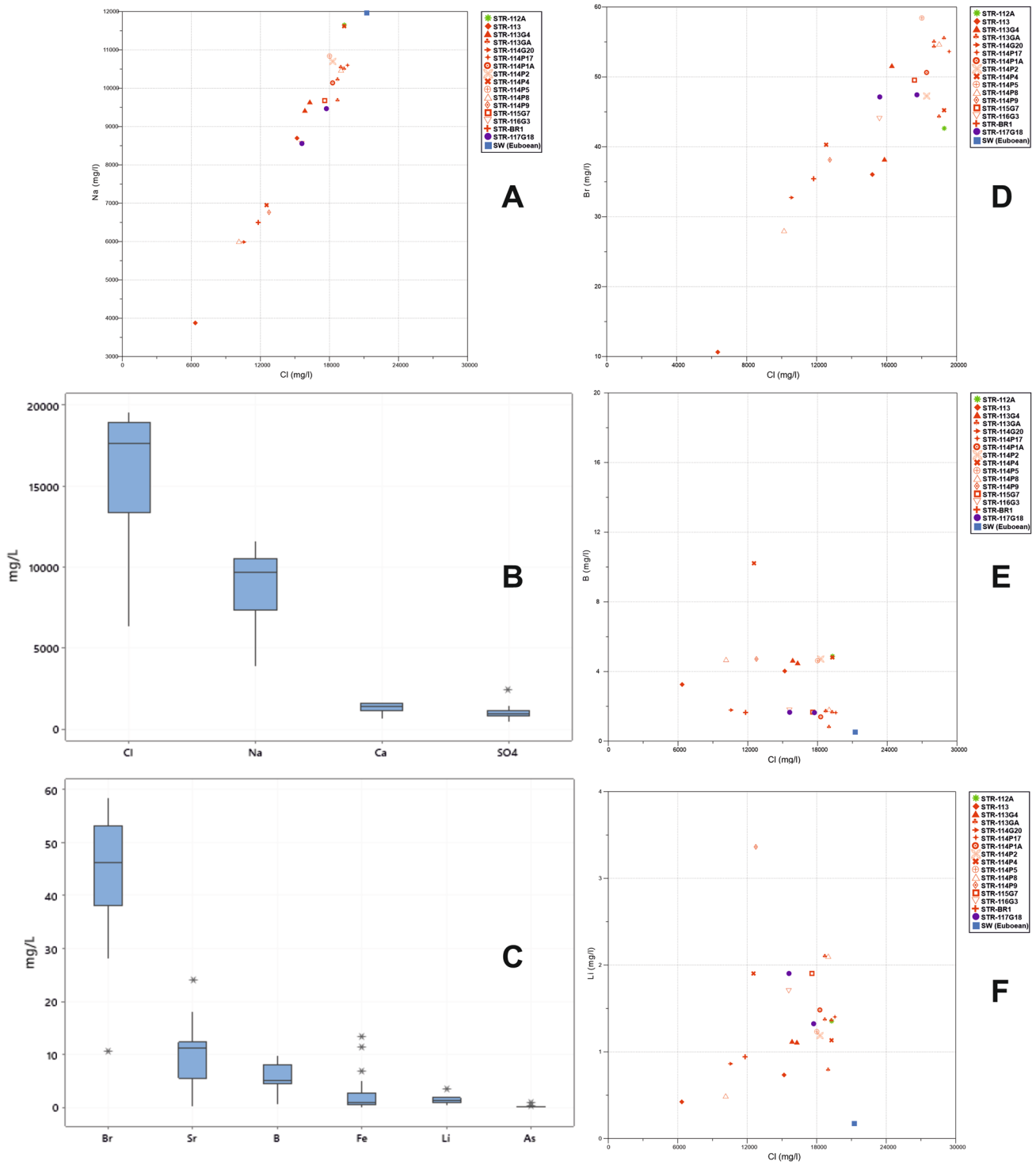

Fig. 5 **a** Chemical composition of the studied geothermal fluid samples from only hot springs and boreholes plotted in Na vs Cl diagram. Box-plots comparing elemental concentration ratios of **b** selected major ions and **c** selected trace elements from only hot springs and boreholes samples. Chemical composition of the studied geothermal fluid samples from only hot springs and boreholes plotted in: **d** Br vs Cl diagram, **e** B vs Cl diagram and **f** Li vs Cl diagram

possible common source of these two elements. Among the conservative constituents, the highest correlation coefficient is between Cl and Br (0.69).

Factor analysis was applied on 24 pairs (springs and boreholes samples) of variables. The correlation matrix of the studied elements was computed after normalization of the

Table 4 Summary statistics of physiochemical and chemical parameters analysed in geothermal fluid samples from only hot springs and boreholes, from NW Euboea Island

	Min	Max	Mean	Median	Stand. Dev. (SD)	Range	Count (N)
Temp. (°C)	43.4	82.2	62.0	61.1	11.5	38.8	24
pH	5.9	6.8	6.3	6.2	0.3	1.0	24
EC (mS/cm)	18850	50230	42161	45565	8338	31380	24
TDS (mg/L)	12550	34970	28550	30730	6080	22420	24
Ca (mg/L)	642	1668	1310	1368	307	1026	24
Mg (mg/L)	140	620.7	276	265.5	102	480.7	24
Na (mg/L)	3870	11641	9039	9653	2025	7771	24
K (mg/L)	110	363	285	306	69	253	24
HCO_3 (mg/L)	265	691	588	611	94	426	24
Cl (mg/L)	6345	19574	16067	17660	3587	13229	24
SO_4 (mg/L)	444	2400	999	967	375	1956	24
NH_4 (mg/L)	0.15	1.93	0.52	0.44	0.34	1.78	24
NO_2 (mg/L)	0.08	5.35	1.28	0.28	2.28	5.27	5
F (mg/L)	3	4.82	4.27	4.49	0.51	1.82	24
SiO_2 (mg/L)	8	102	31.5	18.0	21.0	94	24
As (µg/L)	50	780	130	99	145	730	24
B (µg/L)	547	9720	5697	5130	2443	9173	24
Ba (µg/L)	70	270	195	200	54	200	24
Br (µg/L)	10600	58400	44182	46150	10753	47800	24
Cu (µg/L)	50	205	134	135	45	155	24
Fe (µg/L)	10	13300	2435	950	3470	13290	24
I (µg/L)	150	590	445	427.5	109	440	24
Li (µg/L)	420	3360	1385	1335	629	2940	24
Mn (µg/L)	16	500	137	87	133	484	19
Ni (µg/L)	40	100	77	80	15	60	23
Pb (µg/L)	20	34	25	24	5	14	8
Rb (µg/L)	19	220	150	170	44	201	24
Se (µg/L)	170	480	322	305	87	310	24
Sr (µg/L)	120	24000	9670	11235	5850	23880	24
V (µg/L)	50	150	94	100	30	100	24

variables. This transformation was necessary to meet the assumption of normality in the application of parametric statistical tests. Factor analysis revealed that four main factors are controlling the chemical composition of geothermal fluids (Table 6). The first factor contains K, Mg, Cl, TDS, Br, and Na, with high positive loadings and SO_4 and Ca, with medium positive loadings. This factor is the most important, accounting for 42.3% of the total variance and represents the effect of seawater on geothermal fluid composition. The second factor comprises of B and temperature, with high negative loadings, F and SiO_2, with medium negative loadings. This factor is the second most important, accounting for 18% of the total variance, and it is related to the deep thermal origin of the geothermal fluid and the heat source. The third factor comprises of V, As and Ni, with high to medium positive loadings and accounts for 17.3% of the total variance. This factor represents the influence of ultramafic rocks from the ophiolitic sequence, during the upflow zone of the geothermal fluid circulation. The last factor comprises of Fe with high negative loadings, representing most probably the effect of metamorphic rocks; it accounts for 8.9% of the total variance and represents the influence of these rocks, during the upflow zone of the geothermal fluid circulation.

Additionally, clusters were created, based on the correlation coefficient similarity of the parameters (Fig. 6).

Geothermometry application

Water chemical geothermometers are one of the most important and widely used geochemical tools for the exploration of geothermal systems. They are used for the estimation of sub-surface reservoir temperatures. Water chemical geothermometers are based on the equilibrium of temperature-dependent reactions between minerals and the circulating fluids (Fournier 1973; Giggenbach 1988; Arnórsson 2000).

Since all samples from hot springs and boreholes are characterized as partially equilibrated waters (see Na–K–$\sqrt{Mg}$ diagram, Fig. 4c), cation geothermometers are suitable

Table 5 Correlation matrix of log-transformed physiochemical parameters, major ion and trace elements concentrations for geothermal fluid, from Northwest Euboea

	pH	T	EC	TDS	Li	Na	K	Mg	Ca	Sr	Mn	Fe	NH_4	Ba	Cu	Ni	F	Cl	Br	SO_4	HCO_3	As	Si	B
pH	1.00																							
T	−0.34	1.00																						
EC	−0.14	0.44	1.00																					
TDS	−0.20	0.48	0.95	1.00																				
Li	−0.21	0.43	0.22	0.20	1.00																			
Na	−0.19	0.50	0.82	0.91	0.16	1.00																		
K	0.08	0.48	0.79	0.71	0.40	0.71	1.00																	
Mg	0.14	0.25	0.78	0.68	0.42	0.64	0.93	1.00																
Ca	−0.15	0.42	0.69	0.54	0.45	0.45	0.70	0.69	1.00															
Sr	−0.47	0.35	−0.03	0.06	0.79	0.13	0.07	0.04	0.13	1.00														
Mn	0.07	−0.01	−0.20	−0.26	0.67	−0.29	0.11	0.24	0.38	0.46	1.00													
Fe	−0.50	0.08	−0.03	−0.08	0.33	−0.24	−0.16	−0.14	0.11	0.44	0.14	1.00												
NH_4	−0.12	0.36	−0.15	−0.11	0.24	−0.13	−0.22	−0.32	−0.02	0.37	−0.08	0.35	1.00											
Ba	−0.45	0.60	0.16	0.32	0.26	0.38	0.02	−0.10	−0.02	0.48	−0.45	0.04	0.41	1.00										
Cu	0.06	0.10	0.49	0.46	0.61	0.42	0.62	0.73	0.35	0.36	0.32	−0.08	−0.31	0.14	1.00									
Ni	−0.31	0.23	0.55	0.63	0.51	0.59	0.36	0.40	0.17	0.42	0.04	0.06	−0.12	0.37	0.70	1.00								
F	−0.30	0.73	0.51	0.61	0.20	0.72	0.56	0.31	0.27	0.28	−0.33	−0.16	−0.03	0.59	0.25	0.34	1.00							
Cl	−0.10	0.59	0.91	0.90	0.30	0.89	0.91	0.82	0.64	0.05	−0.13	−0.14	−0.14	0.20	0.50	0.52	0.68	1.00						
Br	−0.05	0.40	0.63	0.59	0.45	0.64	0.76	0.67	0.52	0.32	−0.10	−0.02	0.09	0.33	0.57	0.43	0.53	0.69	1.00					
SO_4	0.13	0.03	0.61	0.60	0.35	0.57	0.67	0.80	0.33	0.10	0.11	−0.27	−0.34	0.05	0.80	0.63	0.23	0.63	0.56	1.00				
HCO_3	−0.43	0.29	−0.10	−0.06	0.36	−0.14	−0.07	−0.19	−0.11	0.51	−0.02	0.79	0.30	0.26	0.04	0.18	0.18	−0.06	0.12	−0.22	1.00			
As	−0.38	0.09	−0.07	0.08	0.32	0.11	−0.31	−0.20	−0.12	0.54	0.02	0.16	0.42	0.58	0.10	0.38	−0.03	−0.15	−0.03	0.08	0.07	1.00		
Si	−0.59	0.24	−0.28	−0.08	−0.02	0.00	−0.55	−0.65	−0.36	0.41	−0.13	0.18	0.37	0.48	−0.44	0.11	0.21	−0.26	−0.32	−0.45	0.24	0.52	1.00	
B	−0.59	0.52	0.07	0.20	0.24	0.26	−0.16	−0.30	0.12	0.54	0.05	0.28	0.46	0.53	−0.31	0.13	0.43	0.08	0.07	−0.28	0.26	0.50	0.82	1.00

Table 6 Varimax component loadings of four factors. Communality and percentage of variance explained for 16 variables ($N = 24$)

Variable	Factor 1	Factor 2	Factor 3	Factor 4	Communality
K	**0.964**	−0.03	−0.168	0.113	0.972
Mg	**0.949**	0.251	−0.049	0.019	0.967
Cl	**0.932**	−0.263	0.047	0.125	0.954
TDS	**0.876**	−0.185	0.241	0.189	0.896
Br	**0.796**	−0.115	0.107	−0.055	0.661
Na	**0.777**	−0.352	0.303	0.267	0.89
SO_4	**0.75**	0.375	0.41	0.186	0.907
Ca	**0.738**	−0.12	−0.206	−0.371	0.739
B	−0.099	**−0.828**	0.352	−0.265	0.889
Temp.	0.364	**−0.813**	−0.099	−0.088	0.811
F	0.497	**−0.724**	0.112	0.284	0.864
SiO_2	−0.456	**−0.703**	0.486	−0.068	0.944
V	0.148	−0.111	**0.883**	0.308	0.909
As	−0.154	−0.178	**0.831**	−0.237	0.802
Ni	0.554	−0.086	**0.713**	−0.044	0.824
Fe	−0.079	−0.108	0.025	**−0.892**	0.814
Variance	6.7669	2.8871	2.7665	1.423	13.8435
% Var	42.3	18	17.3	8.9	86.5

With bold are marked the main loadings of each factor

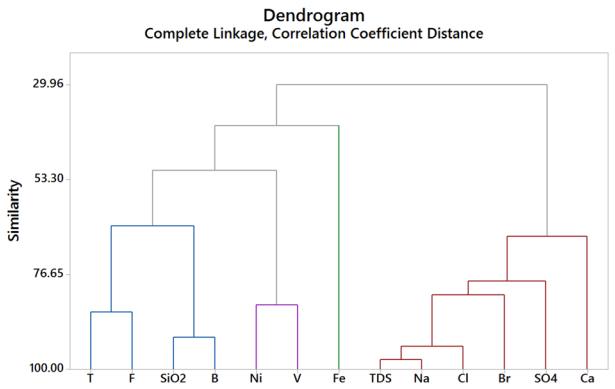

Fig. 6 Dendrogram presenting the correlation coefficient distance between selected physicochemical and chemical parameters of the studied geothermal fluids, from Northwest Euboea

(Giggenbach, 1988). Ten chemical geothermometers, i.e. Mg/Li (Kharaka 1989), Na/Li (Kharaka 1989), Quartz (Fournier 1977), Chalcedony (Fournier 1977), Na–K–Ca, and Na–K–Ca with Mg correction (Fournier 1979), Na–K (Fournier and Potter 1979), Na–K (Truesdell 1976), and Na–K (Fournier 1973) were applied to the geothermal fluids of NW Euboea (Table 7).

The resulting temperatures show significant variations. The estimated temperatures from Mg/Li (Kharaka 1989); Na/Li (Kharaka 1989); Qtz (Fournier 1977), Chalcedony (Fournier 1977) and Na–K–Ca (Mg corrected, Fournier 1979) geothermometers are even lower than the surface measured temperatures.

Water geothermometers, based on dissolved silica content and the solubility of different silica species, are commonly used to estimate the geothermal reservoir temperature (Fournier 1977; Giggenbach,1988; Arnórsson 2000; Wang et al. 2015). The log (SiO_2) versus log (K^2/Mg) diagram (Fig. 7) was applied to indicate which silica species are present in the geothermal fluids and to verify, if such could be used in order to estimate reservoir temperature (Giggenbach et al. 1994; Wang et al. 2015). As shown in Fig. 7, the studied samples are plotted, scattered under the lines of quartz and chalcedony, as they do not control dissolved silica. As can be seen in Table 7, the estimated temperatures using silica geothermometers vary from 32 to 100 °C for Quartz and 17 to 70 °C for Chalcedony. The only exception is the STR-117G18-IL-2 sample (from Ilia), which is plotted on the chalcedony line, with estimated temperatures for Quartz of 138 °C and Chalcedony of 112 °C. For the rest of the samples, in most of the cases, the estimated temperatures are close or even lower than the measured values in the field (Table 7).

The estimated temperatures from the Na/K geothermometer (Truesdell 1976; Fournier 1973) varies from 216 to 243 °C and from 250 to 281 °C, respectively. Only the temperatures derived from the use of Na–K-Ca (Fournier 1979) and Na/K (Fournier and Potter 1979) geothermometers are in a good agreement. Based on the calculations of the Na–K–Ca (Fournier 1979) and Na/K (Fournier and Potter, 1979), water chemical geothermometers, the estimated temperature of the geothermal reservoir is between 140 and 164 °C.

Temperature loggings and geothermal gradient

All the available data from several drilling projects conducted by the Greek Geological Survey focused on northern Euboea Island were collected and re-evaluated. The temperature loggings were conducted after the drilling process and at an equilibrium stage. Based on these, a diagram of temperature loggings vs depth was created (Fig. 8), presenting the temperature loggings of all the geothermal drills at Gialtra (Hatzis et al. 2008), Aedipsos (Voutetakis and Fytikas 1975; Gkioni-Stavropoulou 1998; Hatzis et al. 2008) and Ilia areas (Gkioni-Stavropoulou 1998). In the case of IL-G-18 and AD-G-20 boreholes, the loggings were problematic, and the temperature measurements have to be considered as indicatives (underestimated temp. values, see Gkioni-Stavropoulou 1998), except from the deepest measurements. These two boreholes are artesian, and several repeated field measurements have verified the deep thermal measurements. At the AD-G-3 borehole, which is located near Aedipsos (Agios Nikolaos area),

Table 7 Water chemical geothermometers (°C)

	Temp. (°C, field measurm.)	Mg/Li (Kharaka 1989)	Na/Li (Kharaka 1989)	Qzt (Fournier 1977)	Chalcedony (Fournier 1977)	Na–K-Ca (Mg cor.) (Fournier 1979)	Na–K-Ca (Fournier 1979)	Na/K (Fournier and Potter 1979)	Na/K (Truesdell 1976)	Na/K (Fournier 1973)
STR-112A-01	43.4	35	51	32	–	39	155	153	235	271
STR-113-01	70.1	55	69	57	25	76	158	158	242	279
STR-113-AD-10	71.2	55	63	99	69	81	152	146	225	260
STR-113G4-EOT-1	54.2	55	63	98	68	76	151	144	223	257
STR-113G4-EOT-2	61.9	54	64	97	67	76	151	145	224	259
STR-113GA-01	79.6	55	68	56	24	76	159	158	242	279
STR-113GA-AD-13	78.8	57	64	100	70	77	152	145	224	258
STR-113GA-AD-14	51.3	37	62	83	51	68	141	145	224	259
STR-113GA-EOT-3	80.8	53	59	100	70	76	152	144	223	257
STR-114G20-01	82.2	56	68	56	23	77	158	157	241	279
STR-114P17-KAS-3	55.8	40	54	99	69	80	148	148	228	263
STR-114-P1A-01	69	66	86	56	24	76	157	157	241	279
STR-114P2-2	64.3	64	81	56	24	77	157	157	241	278
STR-114P4-01	58.1	63	82	59	26	76	157	158	242	279
STR-114P4-AD-1	57.3	46	54	92	61	82	152	149	229	264
STR-114P5-01	54.5	56	70	56	23	77	157	157	241	278
STR-114P8-01	60.2	66	85	58	25	76	158	158	242	280
STR-114P8-RK-1	49.2	54	65	98	68	75	151	146	226	260
STR-114P9-01	43.9	51	71	59	27	74	154	157	241	278
STR-115G7-01	71.9	66	82	60	28	36	164	155	237	274
STR-116G3-1	48.7	52	71	50	17	43	160	159	243	281
STR-117G18-01	69.7	83	116	99	69	89	146	150	230	266
STR-117G18-IL-2	63.5	71	93	138	112	95	140	140	216	250
STR-BR1-1	54	51	71	56	24	73	153	156	239	276

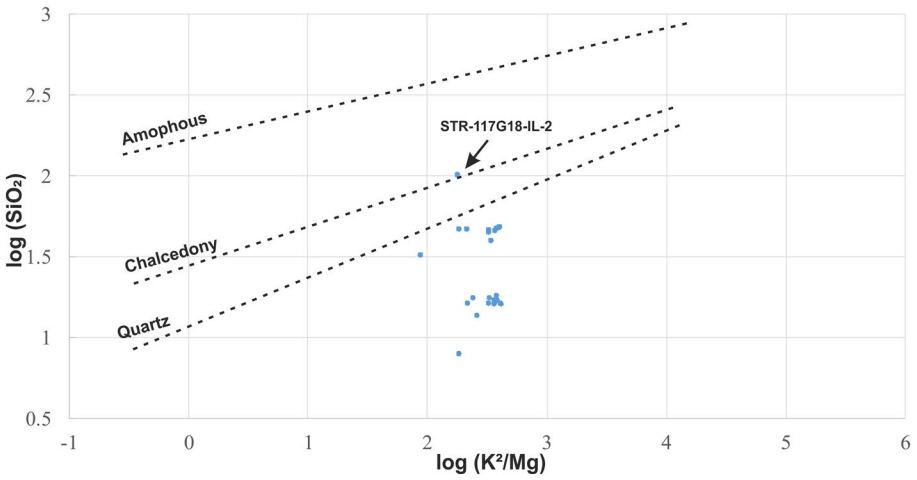

Fig. 7 Plot of log (SiO_2) vs log (K^2/Mg) concentrations in mg/L (Giggenbach and Glover 1992)

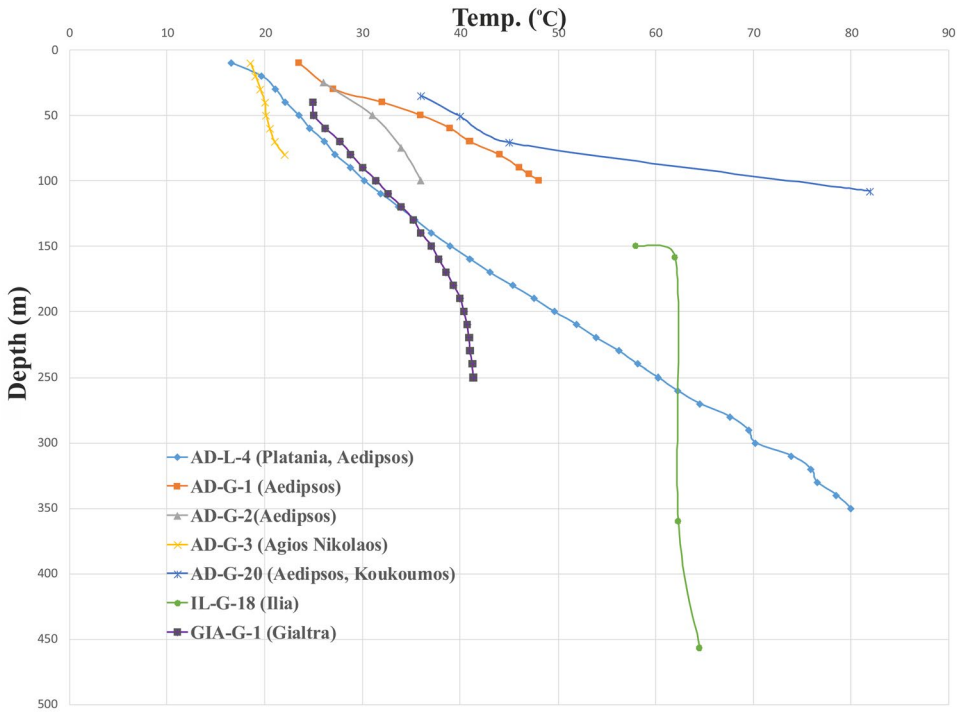

Fig. 8 Temperature logging data of the Northwest Euboean geothermal boreholes

seawater has influenced the borehole, and the temperature measurements were affected by that (Voutetakis and Fytikas 1975).

Based on the evaluated temperature loggings (Fig. 8), in none of them, horizontal temperature increases with depth is observed. By that, it could be conducted that by the drilling projects, no geothermal reservoir was reached.

The cases of very sharp temperature increases with depth, such as AD-G-20 below the upper constant-temperature zone, where possibly small shallow cold aquifers (< 30 m) could occur, suggests that the geothermal fluid enters the borehole laterally from the deeper aquifer, ascends the borehole and flows into the upper part. This fact indicates the high-pressure potential of the deep hot aquifer.

Also, excluding the constant-temperature zone, no negative temperature peaks were identified, which could otherwise suggest permeable geological formations, i.e. potential aquifers. Thus, the metamorphic rock formations, such as gneiss schists, which were identified below Aedipsos and Ilia, are impermeable and function as a geothermal cap. It must be noted that Hatzis et al. (2008), during the drilling of AD-L-4 borehole in-depth 340–350 m, and below a thick layer of gneiss schist (335 m) found a fractured zone within marbles, where geothermal fluid (~ 80 °C) was circulating.

Based on the aforementioned data, the geothermal gradients were calculated for these three areas separately (Table 8). Regarding Aedipsos, where the highest geothermal anomaly has been identified, two geothermal

Table 8 Geothermal gradients

Area	Gialtra		Aedipsos		Aedipsos (Koukoumos)		Ilia	
Code	GIA-G-1		AD-L-4		AD-G-20		IL-G-18	
Reference	Hatzis et al. (2008)		Hatzis et al. (2008)		Gkioni-Stavropoulou (1998)		Gkioni-Stavropoulou (1998)	
	Depth (m)	Temp. (°C)	Depth (m)	Temp. (°C)	Depth (m)	Temp. (°C)	Depth (m)	Temp. (°C)
Depth (constant-temp. zone)	40	24.9	30	20.2	30	20	30	20
Drilling depth	250	41.3	350	80	145	82	457	64.5
Geoth. Grad. (°C/100 m)	7.8		18.7		53.9		10.4	

gradients were calculated. One, based on the AD-L-4 borehole (Hatzis et al. 2008), which is considered to be the most representative for Aedipsos area and one based on AD-G-20 borehole (Gkioni-Stavropoulou 1998), which presents the sharpest temperature increase with depth, i.e. the highest geothermal gradient.

Circulation depth

Since the geothermal reservoirs in the study areas have not identified by drilling, any information or estimation about them, such as the depth of the water circulation, is valuable.

If we accept that i) the temperature of the Aedipsos geothermal fluid is obtained by deep circulation, ii) the temperature is increasing with the depth and iii) the depth of the constant-temperature zone is 30 m, the following equation can suggest the depth of water circulation (Z_{circ}) (Liu et al. 2015; Kanellopoulos et al. 2018a):

$$Z_{cicr} = -\frac{T_r - T_o}{\mathrm{Grad}T} + Z_o,$$

where: T_r = reservoir temperature (in °C); T_o = temperature of initial cold water (in °C); Z_o = depth of the constant-temperature zone (in m) and *Grad*T = temperature gradient (in m/°C).

In the case of NW Euboea, based on the study of Kanellopoulos and Mitropoulos (2013) and using representative samples, the average temperature of the local cold groundwater is assumed to be 14.5 °C. The most representative geothermal gradient is 7.8 °C/100 m for Gialtra, 10.4 °C/100 m for Ilia and 18.7 °C/100 m, for Aedipsos (Table 8). In Aedipsos and specifically in the area of Koukoumos (borehole AD-G-20), there was calculated the anomalous high 53.9 °C/100 m (Table 8), which concerns the STR-114G20-01 sample. For reservoir temperatures, the estimated temperatures of the Na–K-Ca geothermometer (Fournier 1979) are considered as the most representative ones.

So, the estimated circulation depths (Table 9) are: (i) 1831 m for Gialtra, (ii) 1235–1292 m for Ilia and (iii) from 705 to 827 m for Aedipsos area. The only exception is Koukoumos borehole (AD-L-4) with 297 m estimated depth, which could be due to the spatial shape diversity of the geothermal reservoir or a major fault with hot water circulation. These estimations should be used as indicative values until verified by additional methods.

Radiological analyses and residence time

Radiological analyses for ^{222}Rn and ^{226}Ra were conducted, at six representative samples (Table 9). In Aedipsos, four samples were analysed, including Koukoumos (STR-114G20-01), which present anomalous high geothermal gradient. Almost all the studied samples present ^{222}Rn concentrations higher than the parental ^{226}Ra concentrations (Table 9). An exception to this rule is the Koukoumos-Aedipsos and Ilia samples, where high-rate precipitation of thermogenic travertine depositions was identified.

By accepting the hypothesis of a closed system and based on the ^{226}Ra and ^{222}Rn concentrations, the residence time (T_{res}) of the geothermal fluid could be calculated (Cherdyntsev 1971; Zhou et al. 2008; Liu et al. 2015), by applying the following equation:

$$T_{res} = -\frac{1}{\lambda}\ln\left(1 - \frac{N_{Ra}}{N_{Rn}}\right),$$

where: λ = decay constant of ^{226}Ra i.e. 0.00043; N_{Ra} and N_{Rn} = ^{226}Ra and ^{222} Rn contents (in Bq/L), respectively.

The estimated residence time (Table 9) is: (i) for Aedipsos about 18–83 years, with the most represented value being 83 years (see STR-BR1-01 sample, limited travertine deposition); (ii) for Gialtra about 99 years and (iii) for Ilia an unexpectedly anomalous 495 years. These estimations ought to be considered as indicative. In the future, the empirical method of radioactive isotope, tritium, could also be applied, for the estimation of the residence time.

Table 9 Radiological analyses, circulation depth (Z_{circ}) and residence time (T_{res}) of the geothermal fluids

Sample	Locality	Z_{circ} (m)	^{226}Ra (Bq/L)	^{222}Rn (Bq/L)	^{222}Rn/^{226}Ra	T_{res} (years)
STR-113-AD-10	EOT-Ntamaria	763	–	–	–	–
STR-113GA-AD-13	EOT-Artemis	763	–	–	–	–
STR-113GA-EOT-3	EOT-Artemis-Wall	763	–	–	–	–
STR-113GA-AD-14	EOT-Artemis	705	–	–	–	–
STR-117G18-IL-2	Ilia	1234	–	–	–	–
STR-114P4-AD-1	Skourtanioti-Ilios	763	–	–	–	–
STR-114P8-RK-1	Pizou-Kapelari-Cave	758	–	–	–	–
STR-113G4-EOT-2	EOT-G4	758	–	–	–	–
STR-113G4-EOT-1	EOT-G4	758	–	–	–	–
STR-114P17-KAS-3	City Hall-Wall	742	–	–	–	–
STR-113-01	EOT-Ntamaria	795	–	–	–	–
STR-115G7-01	Kompogianni	827	–	–	–	–
STR-112A-01	Gialta	1831	0.73	17.45	23.9	99
STR-113GA-01	EOT-Artemis	801	–	–	–	–
STR-117G18-01	Ilia	1292	0.24	1.25	5.2	496
STR-114P2-2	Skourtanioti-Frini	790	–	–	–	–
STR-114P4-01	Skourtanioti-Ilios	790	–	–	–	–
STR-114P5-01	Ai pigai	790	–	–	–	–
STR-114P8-01	Pizou-Kapelari-Wall	795	–	–	–	–
STR-114P9-01	Papaioannou	774	1.38	67.4	48.8	48
STR-114P1A-01	Thermopotamos	790	–	–	–	–
STR-114G20-01	Koukoumos	297	8.03	7.52	0.9	cannot be calc. (Ra > Rn)
STR-BR1-1	Vrysakia	769	1.66	47.53	28.6	83
STR-116G3-1	Thermae Sylla	806	0.22	28.51	129.6	18

Travertines mineralogy and geochemistry

Based on optical microscopy and XRD analysis of the Aedipsos' travertine depositions, the main mineral phases of the travertines are calcite and aragonite and minor mineral phases are halite and gypsum. Usually, halite crystals were developed at the rims of the pores of travertine.

Whole-rock geochemical analyses in travertine samples from Aedipsos are presented in Table 10. The travertines from Aedipsos contain high concentrations in several major and trace elements such as Ca, Na, S, Ba, Fe, K, Mg, Sr, Si and Zn, and they are reflecting the geochemical composition of the hot spring of the area.

Structural and magmatic settings of the hot springs

Based on a thorough re-evaluation of all the published data concerning especially the magmatic setting (Georgalas 1938, 1940; Gidarikos 1938; Katsikatsos et al. 1982; Pe-Piper and Piper 2002, Kanellopoulos et al. 2019b) and the tectonic setting of the area (IGME, 1957, 1984, 1991; Tzitziras and Ilias 1996; Galanakis 1997; Vakalopoulos et al. 2000; Vavassis 2001; Sakellariou et al. 2007; Hatzis et al. 2008), alongside with field observations, an assessment of the relation between the Euboeas' hot springs and the magmatic and structural setting of each area took place.

In the greater NW Euboea area, only the Plio-Pleistocene Lichades volcanic centre could be related to the studied geothermal system. The Lichades islands, which are located only a few hundred meters from the Euboea coast, consist totally by trachyandesitic lava flows (Fig. 2a). The rest of the volcano-magmatic rock formations in NW Euboea are too old, i.e. Permian–Triassic age. Additionally, some areas, with strong alterations, possibly hydrothermal, were identified. For example, alterations areas were identified in Ilia area, where there is a hot spring nearby, as well as in Agios area, where there is no hot spring in the area.

As far as structural setting concerns, the hot spring at Ilia is located on a marked bend of the marginal fault system, where the average strike changes from SE–NW to E–W (or ENE–WSW). Towards the western tip of the offshore ESE-WNW striking Telethrio Fault (TF), the faults bifurcate into two splays, which can be traced onshore (Fig. 2a). West of Ilia, the southern splay changes its strike towards WSW. This

Table 10 Whole-rock travertine chemistry

	TR-1	TR-2	TR-3	TR-4	TR-5
Ca (%)	36.8	35.0	31.0	35.7	34.4
Na (%)	0.43	0.80	1.77	0.56	1.68
S (%)	0.19	0.32	0.52	0.04	0.38
Al (mg/kg)	94	77	64	bdl	Bdl
B (mg/kg)	27	27	50	12	34
Ba (mg/kg)	140	140	62	3	114
Fe (mg/kg)	368	538	7932	969	1750
K (mg/kg)	263	425	948	757	783
Mg (mg/kg)	220	346	1148	1025	733
Mn (mg/kg)	2	2	12	71	6
P (mg/kg)	32	37	29	bdl	bdl
Sr (mg/kg)	3360	3650	3200	625	3620
Si (mg/kg)	933	832	611	79	702
Zn (mg/kg)	6.65	3.20	3.87	6.73	bdl
As (µg/kg)	bdl	bdl	bdl	bdl	bdl
Be (µg/kg)	141	311	1411	405	544
Cd (µg/kg)	8	5	10	11	17
Co (µg/kg)	bdl	bdl	bdl	bdl	bdl
Cr (µg/kg)	bdl	bdl	bdl	bdl	bdl
Cs (µg/kg)	117	324	1139	673	600
Cu (µg/kg)	bdl	bdl	bdl	bdl	bdl
Hf (µg/kg)	56	47	20	bdl	31
Li (µg/kg)	844	1700	3896	2257	2675
Ni (µg/kg)	bdl	bdl	bdl	bdl	bdl
Pb (µg/kg)	421	bld	942	1664	bdl
Sb (µg/kg)	47	51	283	678	89
Sn (µg/kg)	bdl	107	bdl	bdl	bdl
Th (µg/kg)	7	2	14	5	3
Ti (µg/kg)	bdl	bdl	1619	bdl	bdl
U (µg/kg)	12	14	13	7	14
Y (µg/kg)	643	64	163	659	85
Zr (µg/kg)	2085	1660	576	98	817

bdl = below detection limit

may be related to either an inherent old tectonic structure, or to an ENE–WSW to E–W neotectonics fault (Ilia Fault—IF, Fig. 2). The IF connects two overlapping SE–NW segments of the coastal fault system, i.e. TF and AF. Therefore, the Ilia hot spring is sited at the intersection of these two fault systems, near the seashore.

Aedipsos is located close to the termination of the namesake SE–NW Aedipsos Fault (AF) that runs adjacent to the coast and appears to die out within the Aedipsos Gulf. Field reconnaissance and detailed mapping onshore show that several faults are mapped in the area, belonging to the footwall of the coastal fault system. A group of sub-parallel close-spaced minor ENE–WSW parallel faults are mapped east of Aedipsos, while NE–SW faults are mapped mainly at the eastern and north-eastern parts of the town (Fig. 3a). The continuity of some of these faults is obscured by the travertine deposits, but they can be clearly mapped in the outskirts of Aedipsos (Tzitziras and Ilias 1996; Vavassis 2001).

These intersecting structures form a dense fault network that is probably related to the faulting process at the termination of the AF, which involves the development of minor faults that accommodate the deformation close to the fault tip. Therefore, the hot springs of Aedipsos are situated within a broad damage zone, at the tip of the Aedipsos Fault.

Karastathis and Mouzakiotis (2014), based on offshore seismic data, suggest that the Gialtra hot spring could be controlled by a NE–SW fault, which follows the bathymetry of the area and continues onshore below the Post-Alpine sediments (Galanakis 1997). However, the presence of the E–W striking Lichades Fault System (LFS, Fig. 2; IGME 1991) also plays a role, controlling the morphology of the coastline. Thus, the Gialtra hot spring is related to the intersection of these two fault systems, near the seashore.

Spatial distribution of temperature and near-surface thermal anomalies

To visualize the spatial distribution of the shallow geothermal fluid circulation temperature in the Aedipsos area, a surface temperature interpolation map was produced (Fig. 9), by applying the Kriging interpolation method. Based on the field measurements, the temperatures of the hot springs ranged from 43 to 69 °C, and the temperatures of the artesian boreholes ranged from 44 °C to 82 °C. The submarine hot springs showed temperature between 27 and 33 °C.

Based on the spatial distribution of the shallow geothermal fluid circulation temperatures (Fig. 9), the maxima were detected at the intersection of the three fault systems in the area, i.e. (i) NNE–SSW to NE–SW, (ii) ENE–WSW to E–W and (iii) NNW–ESE to NW–SE. Also, a thermal anomaly (Fig. 9) suggests the occurrence of NNE–SSW faulting running through the south-eastern part of the town, beneath the thermogenic travertine deposits.

To investigate and visualize the terrestrial, sea-surface and submarine thermal anomalies, thermal infrared images were taken (Fig. 10). Based on these, the existence of at least two submarine hot springs (Fig. 10a, b, e and f) were documented for the first time, in the area of Aedipsos. In many cases, thermal anomalies (hot plumes) were identified at the sea-surface, as the result discharges of terrestrial and submarine hot springs discharges (Fig. 10a, b, e and f).

The temperature of the terrestrial hot springs/artesian boreholes goes up to 84 °C (Fig. 10c, d). The thermogenic travertine depositions of Aedipsos have high temperatures in several locations since hot water circulates inside them (shallow circulation). Characteristic examples are when water emerges from stone walls, used to retain the travertine mass

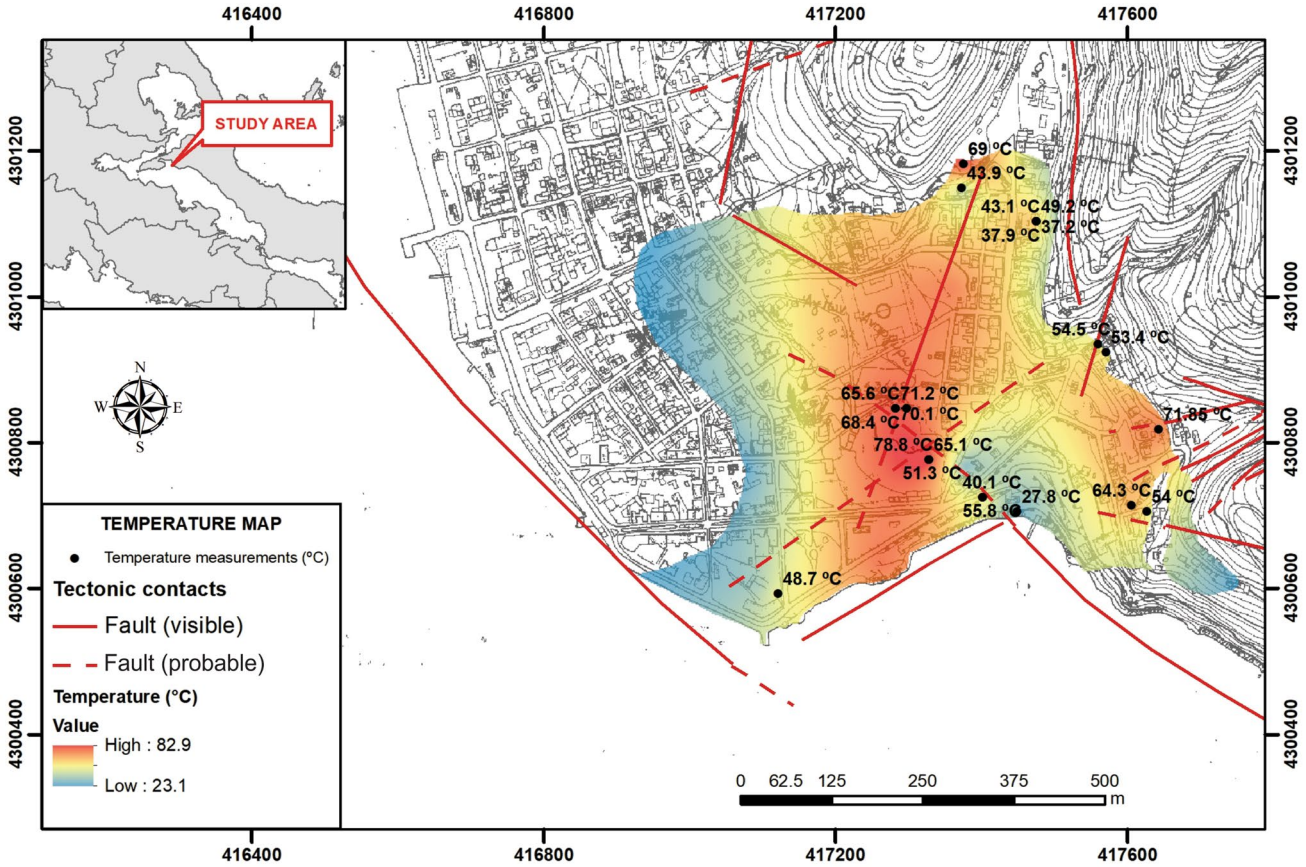

Fig. 9 Surface temperature distribution, based on the hot springs and shallow boreholes (> 40 m) of the Aedipsos area. The geographical coordinates are in EGSA '87

on its sides (Fig. 10g) and the identified thermal anomalies in the inside walls of the Roman thermal baths (Fig. 10h, i).

Discussion and conclusions

In the northwestern Euboea (Evia) Island, hot springs occur in three areas: (i) Gialtra, (ii) Aedipsos and (iii) Ilia. The main hot springs occurrences in the northwest of the island are located in Aedipsos area. In Gialtra and Ilia, only one hot spring occurs in each area. Euboea has been recognized as an area with the highest geothermal gradients in Greece, just after the south Aegean active volcanic arc (Fytikas and Kolios 1979), but the geothermal heat capacity of the area has not been exploited yet (Kanellopoulos et al. 2017b).

Seawater-dominated geothermal systems, such as Euboea's, are of high importance since they are proposed as analogues for seafloor massive sulfide deposits. Recent studies have demonstrated the metal content and ways of transfer in these systems (Hardardóttir et al. 2013; Hannington et al. 2016; Grant et al. 2019; Hannington and Garbe-Schönberg 2019). Kanellopoulos et al. (2017a, 2018b) have suggested the Euboea hydrothermal system as a new terrestrial active mineralizing hydrothermal system associated with ore-bearing travertines. Since, they identified sulfides (pyrite, arsenopyrite, galena, chalcopyrite, sphalerite, stibnite), native elements such as Fe (Kanellopoulos et al. 2018b), alloys like Au ± Cu–Ag, fluorite and REE-bearing phases, syngenetically enclosed within the pores of thermogenic travertines and ferrihydrite deposited at the surface. The presence of ferrihydrite-rich travertine, at an ore-grade concentration (up to 35.3 wt% Fe), Kanellopoulos et al. (2019a) after geological and geomicrobiological studies suggested that presents pre-diagenesis facies association and mineralogy that could bring new clues for unravelling "Banded Iron Formation" (BIF) modes of formation and the salient biogeochemical conditions characteristic of their original depositional environment. Additionally, deposition of travertine from terrestrial seawater-dominated hot springs are also rare (Kanellopoulos et al. 2017a) and adds even more scientific importance to the Euboea geothermal system.

Based on a series of mineralogical and geochemical observations Kanellopoulos et al. (2017a, b) suggested that metals, native iron and metalloids in the study area were

mainly derived from magmatic fluids, which after mixing with heated seawater deposited sulfide mineralization at depth, and As-enriched hydrous iron oxides in the studied travertines at the surface. Also, they support the hypothesis that there is a remobilization from carbonate-hosted sulfide mineralization and suggest that the study area has potential for a future base and precious metal discoveries.

The findings mentioned above suggest the high-importance of understanding the Euboea's geothermal fluids, and especially their controlling factors and their underground circulation, since only few information are known.

Geothermal fluid chemistry and travertine deposition

The Euboea hot springs vary in temperature from about 44–84 °C, with their maxima at the Aedipsos hot springs/artesian boreholes, as well as the maxima fluid discharge. All samples are classified as near-neutral pH, Na–Cl fluids (Table 1). They have a very close chemical relation between them, indicative is the limited distribution of the studied samples on the Piper characterisation diagram (Fig. 4a). That implies that most probably the studied fluids have a common origin and they do not change their chemical composition significantly during their upper part of ascent, i.e. no or limited mixing processes with local cold aquifers and the meteoric water.

Additionally, the comparison between samples from different sampling periods (dry and rain period) revealed only limited concentration variations in trace elements, suggesting only limited participation of meteoric water in the studied system. Previous studies have also identified only small variations in the hydrochemical characteristics of the studied fluids, between different sampling periods (Kanellopoulos et al. 2017a).

High concentrations of Cl (up to 1.96%), Na (up to 1.16%) and a series of elements (conservative constituents, Tables 2, 3) such as F, B, SiO_2, Br and Li were detected, which could be associated with seawater and/or are likely to be of a deep geothermal fluid member.

Almost all samples present excess to B and Li compared to seawater, suggesting additional water–rock interactions and/or mixing with a deep geothermal fluid member. Similarly, in most cases, ratios such as Br/Cl, K/Cl, Na/Cl, Ca/Cl and Li/Cl (Table 2) are higher than or near the seawater value, supporting the hypothesis that the very high salinity represents high seawater participation and additionally secondary processes like water–rock interactions and/or mixing with a deep geothermal fluid member. Taking into account, the geological formations present in the area, the excess of B, compared to seawater, could originate from sediments. Bebout et al. (1993) have shown that B loss from sediments is strongly related to the heating during fluid circulation. However, the high Li/B ratio presents a wide variability from 0.01 to 0.12, typical of water discharged from 'rift-type' and 'arc-type' systems (Giggenbach et al. 1995). Similar ratio variations have reported in the Nisyros geothermal fluids (0.05–0.18; Marini and Fiebig, 2005), indicating correspondences between the geothermal system of Euboea and volcanic-related geothermal systems. Thus, a relation between the studied system and the neighbouring Lichades volcanic centre may be proposed. Dotsika (2015) suggests that the supply of B and Li is closely related to rock leaching and reflects to a great extent the alteration to the geothermal fluids by the crustal zone during the submerging and the resurfacing of the fluids. It must be noted that the intensity of the fluid–rock exchange depends, besides other factors, on the relative proportions of fluid and rocks, of the surface area and the duration of contact.

The HCO_3/Cl ratios (Table 2) of the studied geothermal fluids are even 10 times higher compared to seawater. At the same time, the HCO_3 concentration is two to three times higher than the local cold groundwaters (Kanellopoulos and Mitropoulos 2013), suggesting that the geothermal fluids are enriched due to water–rock interactions (Stober and Bucher 2002).

The Ca/Cl, and Mg/Cl ratios (Table 2) of the studied geothermal fluids are both rather higher and lower compared to the seawater, respectively, suggesting possible interaction of the geothermal fluids with deep volcanic formations under high temperatures and CO_2 pressures (Dotsika 2015). At high temperatures, Mg^{2+} is incorporated into secondary alteration minerals by ion exchange reaction (Nicholson 1993), stripping the solution of its Mg^{2+} contents. The high Ca contents could be attributed to an equilibrium with a hydrothermal mineral (Na–K-feldspar, calcite, muscovite) at high temperatures and CO_2 pressures (Truesdell et al. 1981) and from limestones/marbles dissolution.

The aforementioned data combined with isotopic results from other studies (Mitropoulos and Kita 1997; D'Alessandro et al. 2014; Dotsika 2015) strongly suggests high seawater participation in the deep part of the system. Additionally, their Cl–SO_4–HCO_3 and Na–K–$\sqrt{Mg}$ correlations (Fig. 6) suggest that the studied fluids are deep waters with volcanic origin affinities, which are partially equilibrated with the minerals of the geothermal reservoir.

Also, high concentrations in conservative constituents such as Br (up to 58.4 mg/L), Li (up to 3.36 mg/L), as well as relevant ion ratios, combined with water and gas isotopic results (Shimizu et al. 2005; D'Alessandro et al. 2014; Dotsika 2015) suggest that the studied hot springs are fed by a deep parent geothermal fluid, mixed with seawater. They present similarities with geothermal systems of the south Aegean active volcanic arc, highlighting the relation between the studied system to the volcanic centre of Lichades and the associated magma chamber. The Aedipsos

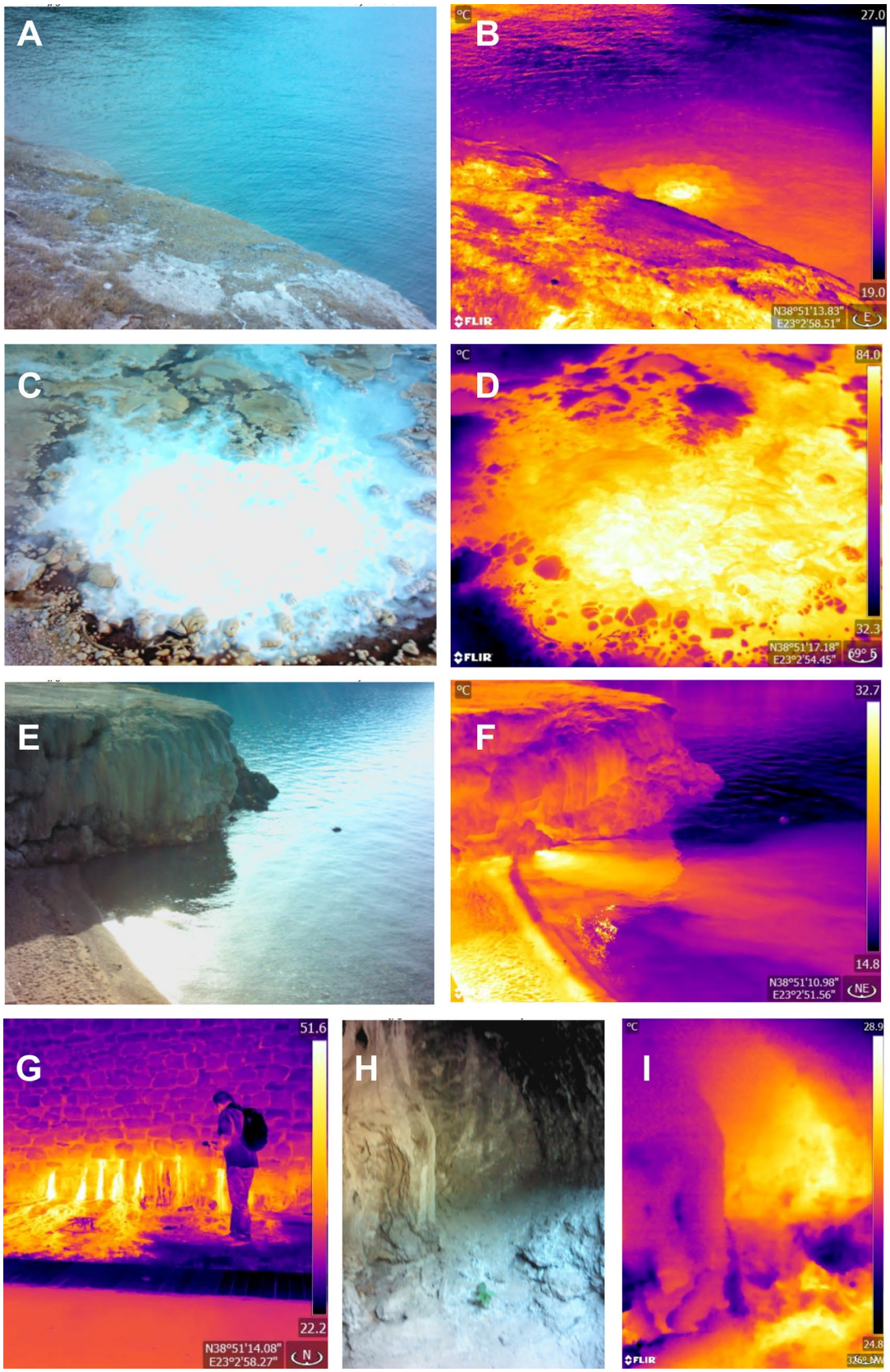
A
B
°C
27.0
19.0
FLIR
N38°51'13.83"
E23°2'58.51"
C
D
°C
84.0
32.3
FLIR
N38°51'17.18"
E23°2'54.45"
E
F
°C
32.7
14.8
N38°51'10.98"
E23°2'51.56"
NE
G
51.6
22.2
N38°51'14.08"
E23°2'58.27"
N
H
I
°C
28.9
24.8
FLIR

◂**Fig. 10** Paired views of the Aedipsos hot springs: normal image and corresponding thermal image of the same area. At the right side of each thermal picture, a colour column shows the temperature scale corresponding to the colours. **a**, **b** Offshore hot spring, creating thermal anomaly (halo). **c**, **d** Artesian hot borehole with temperature up to 84 °C. **e**, **f** Offshore hot spring discharging at the base of a thermogenic travertine cape, and the spring's hot plume in the sea. **g** Hot water emerging from a retaining stone wall, used for supporting the side of a travertine mass. **h**, **i** Thermal anomaly inside the clogged Roman Thermal Baths

He gas isotopes present a positive anomaly (enrichment) in mantle He ($^3He/^4He \sim 1\ R_A$, Shimizu et al. 2005), resembling the south Aegean active volcanic arc related hot springs.

Based on the correlation coefficients, factor and cluster analysis, the chemical composition of the geothermal fluids is controlled by four factors. The most important factor, accounting for 42.3% of the total variance, represents the effect of seawater on geothermal fluid composition, i.e. the main source of the geothermal fluid. The second factor, accounting for 18%, is related with the deep thermal origin of the geothermal fluid and the heat source. As far as concerns the third factor, it is comprised of V, As and Ni, accounting for 17.3%. It is related with the co-variation and the concentrations of Ni and Cu. It must be noted that seawater-dominated geothermal systems are enriched to these elements. Although, as concerns NW Euboea, Kanellopoulos and Argyraki (2013) and Kanellopoulos and Mitropoulos (2013) have proven that elements like V, Ni, Cr, Cu are present in noticeable concentrations in the soil and the cold groundwater aquifers of the NW Euboea and they are related with the local ultramafic rocks from the ophiolitic sequence. Thus, taking under consideration the geological data of the study area and the fact that factor analysis separated these elements as a separate factor, it is suggested that their enrichment is the result of the ultramafic rocks from the ophiolitic sequence influence, during the upflow zone of the geothermal fluid circulation. The last factor is related to the influence of the metamorphic rocks, during the upflow zone of the geothermal fluid circulation.

The large deposits of thermogenic travertine (Table 10), especially in Aedipsos (Kanellopoulos 2011, 2013), and the high Ca concentrations of the fluids (Table 2), strongly suggest that the geothermal fluids at some point meet and dissolve carbonate rocks. Based on the drilling data (Gkioni-Stavropoulou 1998; Hatzis et al. 2008), marbles and limestones are present as bedrock below Aedipsos. The AD-L-4 borehole (Hatzis et al. 2008) encountered marbles at a depth of 340–350 m. Within these marbles, a fractured zone was identified, with a circulation of geothermal fluids (~ 80 °C). Thus, the geothermal fluid enriches in Ca, by dissolving the bedrock carbonates of the area and deposits thermogenic travertine, at the surface due to pressure and temperature change.

In several cases, the Aedipsos hot springs present intense bubbling, as a result of degassing, indicating high gas pressure in the geothermal system. Most probably, the gas phase separates at depth, leaving a dissolved gas phase that is progressively depleted in the less soluble gases (i.e. He and N_2). This residual phase is finally separated from the fluid at shallow depths or at the emerging point. D'Alessandro et al. (2014) after analysing the chemical and isotopic composition of the gas phases, concluded that Aedipsos and Ilia are CO_2-dominated, while at Gialtra, they are N-dominated. Based on that, the limited to non-presence of travertines to Gialtra area could be explained, in contrast to Aedipsos and Ilia areas. Since travertine precipitation results primarily through the degassing of CO_2 from the groundwater, leading to calcium carbonate supersaturation. The isotope composition of CH_4 indicated a hydrothermal origin (possibly abiogenic, D'Alessandro et al. 2014). The obtained CO_2 isotopic composition was found to be similar to the samples from the south Aegean active volcanic arc (D'Alessandro et al. 2010, 2014; Parks et al. 2013) and suggested that were a result of mixing between CO_2 of mantle origin with CO_2 deriving from marine carbonate thermal metamorphism (i.e. decarbonation of marine limestone within the crust at an estimated depth < 8 km).

Structural and magmatic control on hot spring formation and new areas of geothermal interest

Based on the aforementioned data, the Plio-Pleistocene Lichades volcanic centre is related to the studied geothermal system. Taking into consideration, the existence of a magmatic chamber at about 7–8 km depth below the Euboean Gulf (Karastathis et al. 2011), it could be suggested that this magmatic chamber could be the main heat source of the geothermal system. Also, areas with possible hydrothermal alterations in the study area, ought to be studied in the future, since they could be related to hidden geothermal resources.

As it was mentioned above, ancient historians such as Thucydides and Strabo, as well as modern scientists (Pertessis 1937; Margomenou-Leonidopoulou 1976) described observations about the effect of strong historical earthquakes on the occurrence of Northern Euboeas' hot springs. All this information is indicative of the relation between seismicity/tectonic setting and the presence of the studied hot-springs. Studies performed in tectonically active geothermal areas revealed that fault surfaces are preferential fluid pathways, where the pressure and temperature of the field is significantly different. The fault surfaces play a significant part in the recharge or discharge of the reservoir (e.g. Arnorsson 1985; McGuinness et al. 1995; Banks et al. 1996; Caine et al. 1996; Magri et al. 2010; Cherubini et al. 2013).

Additionally, in the present study, submarine hot springs were documented for the first time in the area (Fig. 10a, b, e and f), suggesting the continuation of the geothermal field manifestations into the seafloor of the North Euboean Gulf. It is not clear yet if offshore hot springs connect the main hot spring areas in NW Euboea and the mainland (Sperchios). The presence of hot springs near the seaside at both sides of the Northern Euboean Gulf, i.e. Euboea: Aedipsos, Ilia and Gialtra and mainland, i.e. Kamena Vourla, leaves that question open. Until now, in Greece, submarine hot springs with corresponding hydrothermal depositions, such as hydrothermal chimneys and hydrothermal metallic sedimentation, have been identified only in the seafloor of the South Aegean active volcanic arc (e.g. Valsami-Jones et al. 2005; Price et al. 2013; Kilias et al. 2013; Kati et al. 2015). The submarine hot fluid discharges could create locally noticeable thermal anomalies, with high concentrations in a series of metallic and other elements, creating unique extreme environments, where rare biomineralization processes could take place. Kanellopoulos (2014) and Kanellopoulos et al. (2015; 2019a) have already discussed the presence of biomineralization processes in the terrestrial hot springs of NW Euboea and Sperchios, respectively.

All the hot springs in NW Euboea are located at the junctions of two or three fault systems. Even though, it seems that they are developed in an NW–SE direction, similar to the marginal fault on the south coast of the Northern Euboean Gulf, the main fault strikes in all areas are the E–W to ENE–WSW ones, with Oreoi Strait being sited at the possible extremity of the North Anatolian Fault. Spring occurrences in the study area can be related to lateral tips of a major fault segment, with the presence of complex networks of additional fault systems leading to fault intersections.

The hot spring of Ilia area is located on a marked bend of the marginal fault system, where the SE–NW offshore Telethrio Fault (TF) splits into two splays, one SE–NW which can be traced onshore and another since the fault strike swings to the ENE–WSW to E–W fault (Ilia Fault—IF, Fig. 2a). The hot spring of Gialtra is related to the intersection of the NE–SW fault, which follows the bathymetry of the area and the E-W striking Lichades Fault System (LFS, Fig. 2a), which is controlling the morphology of the coastline. In the case of Aedipsos, three fault systems are present: (i) the major NW-trending front fault, controlling the south part of Northern Euboean Gulf and the relevant coastline, (ii) the E–W to ENE–WSW fault system, controlling the Oreoi Strait and (iii) the NNE–SSW to NE–SW system, which is mapped onshore (Tzitziras and Ilias 1996; Vavassis 2001; Figs. 2a and 3). Based on the tectonic data and the spatial distribution of temperatures (Fig. 9), it seems that the main hot springs occur near fault intersections, mainly between the ENE–WSW and NNE–SSW fault systems and in some cases between also the NW–SE fault system. These intersecting structures form a dense fault network that is probably related to faulting processes operating at the termination of the Aedipsos Fault (AF), which involve the development of minor faults that accommodate the deformation close to the fault tip. Therefore, the hot springs of Aedipsos are situated within a broad damage zone, at the tip of the Aedipsos Fault. This conclusion is also supported by the travitonics data, i.e. the combination of thermogenic travertine depositions and structural data (McGarth and Davison 1995; Hancock et al. 1999), since the most characteristic morphological types of the travertine deposits of the area are terraces and mounds (Kanellopoulos 2012, 2013). To characterize them further as either "locked fault interactions" or as "slipping fault-intersections" (Curewitz and Karson 1997), more detailed structural and tectonic study of the area is needed.

The understanding of the magmatic processes and tectonic control on the hot springs and the thermal anomaly of the greater area is of the great importance of any future exploration project. Since, they could suggest areas with hidden geothermal resources, i.e. areas without surface manifestations, similar to Ampelia area, Eastern Thessaly-Greece (Kanellopoulos et al. 2016). For example, the area at the direction NNE–SSW to NE–SW from Aedipsos is promising to include hidden geothermal resource locations.

Sub-surface and reservoir characteristics

Even though geothermal drilling projects have been conducted on NW Euboea Island, the geothermal reservoirs have not been identified yet. Therefore, any information that could be conducted by assessing all the available information is highly valuable.

Since the water samples are characterized as partially equilibrated waters (Fig. 4c), numerous water chemical geothermometers were applied to estimate the temperatures of the reservoirs. Several geothermometers estimate temperatures lower than the surface measured temperatures. As regards the Mg/Li and Na/Li geothermometers, they are problematic, since Li is a minor constituent in the studied geothermal fluids, while Na and Mg are major. As a result, slight changes in Li concentrations during the ascent of the fluid significantly affect the Na/Li and Mg/Li ratios. The estimated temperatures of Mg-involving geothermometers are low. That could be explained since the studied fluids have low Mg concentrations, so relatively limited reaction in the upflow with side-rocks could alter the aqueous Mg concentration significantly (Arnórsson 2000). The estimated temperatures by the silica geothermometers are close or even lower than the measured values in the field (Table 7). The only exception is the Ilia sample (STR-117G18-IL-2), with estimated temperatures for Quartz: 138 °C and for Chalcedony: 112 °C. The Na/K (Truesdell, 1976) and Na/K

(Fournier, 1973) water chemical geothermometers are suggesting temperatures from 216 to 243 °C and from 250 to 281 °C, respectively. Dotsika (2015), by applying isotopic geothermometers [$\delta^{18}O$ (SO_4–H_2O)] at hot springs of Aedipsos, calculated temperatures between 230 and 240 °C and suggests as possibly more representative a temperature close to 200 °C. So, these estimations are in agreement. Also, the use of ratios such as Na/K and Na/K, instead of absolute abundances of the ions, makes the Na–K geothermometers less sensitive to any secondary processes, such as mixing and boiling, which could change the original characteristics of the geothermal fluid. But, in the case of diluted water or a system below 150 °C, this often results in an overestimation of the calculated temperature (Henley et al. 1984; D'Amore et al. 1987; Wang et al. 2015). This is because Na/K ratio of water at low temperatures is governed by leaching rather than chemical equilibrium, which goes against the basic assumption for a chemical geothermometer application. Also, high Ca contents in geothermal fluids, as in these of NW Euboea, may also lead to unreasonably high-temperature estimates by Na–K geothermometers (Fournier and Truesdell 1973).

Based on the evaluation of the applied water chemical geothermometers and considering all the available data about the geology of the area, the derived temperatures from Na–K-Ca (Fournier 1979) and Na/K (Fournier and Potter, 1979) geothermometers, which are in a good agreement, are considered as the most appropriate from the NW Euboea system. Since the Na–K-Ca geothermometer was formulated for fluids containing relatively high calcium, it assumes that a fluid mineral equilibrium is established between Na and K feldspars, calcic minerals (calcium feldspar, epidote, calcite) and clay minerals, which are common in the metamorphic rocks of the local bedrocks. So, these geothermometers seem to be the more suitable for Euboea geothermal fluids. Based on these estimations, the geothermal reservoir is between 140 and 164 °C. Although, multicomponent geothermometric tools such as RTEst (Palmer et al. 2014) and GeoT (Spycher et al. 2014), which are based on complete fluid analyses and a solid thermodynamic basis, should be applied in the future to verify this point or to suggest a more accurate geothermal reservoir temperature.

Based on the radiological analyses, most of the samples present ^{222}Rn concentrations higher than the parental ^{226}Ra concentrations (Table 9). The ^{222}Rn is inactive and an easily dissoluble gas. The low imbalance of $^{222}Rn/^{226}Ra$ ratios suggests that the dissolved ^{222}Rn emanates mostly from the decay of the parental ^{226}Ra of the fluid and that there is only limited enrichment from the surrounding rocks. In the areas where thermogenic travertine is being deposited, the ratio of $^{222}Rn/^{226}Ra$ is very low, even < 1. Characteristic cases are Koukoumos (STR-114G20-01), Ilia (STR-117G18-01), Artemis (STR-113GA-AD-13) and Ntamaria (STR-113-AD-10) artesian boreholes (see radiological analyses from Athanasoulis et al. 2009, 2016; Kanellopoulos et al. 2018a). Koukoumos (STR-114G20-01) has 8.03 Bq/L ^{226}Ra, which is among the highest ^{226}Ra concentrations in Greek hot springs (Athanasoulis et al. 2009, 2016; Kanellopoulos et al. 2018a), but at the same time is very close to the relevant ^{222}Rn concentration. Most probably, the low concentrations of ^{226}Ra (related to ^{222}Rn) could be attributed to the presence of high concentrations of SO_4^{2-} and Ca^{+}, as suggested by Lopez (Lopez et al. 2004). The presence of these ions in concentrations close to the $CaSO_4$ solubility degree causes precipitation of the $CaSO_4$ and consequently parallel co-precipitation the $RaSO_4$. Additionally, ^{226}Ra could easily substitutes for Ca in gypsum (Godinez et al. 1997; Yoshida et al. 2009; IAEA 2014) which is present in the local travertines (Kanellopoulos 2011; Kanellopoulos et al. 2017a).

By applying the ^{226}Ra–^{222}Rn method, it was estimated that in most cases the geothermal fluids took around 80–100 years to flow from the recharge areas to the discharge points in NW Euboea. The estimated circulation depths vary from about 1830 m for Gialtra, 1230–1300 m for Ilia and 700–830 m for Aedipsos. These estimations agree with Kanellopoulos et al. (2018a) results. In the case of Koukoumos area (AD-L-4 borehole, max. geoth. gradient), the estimated circulation depth is only about 300 m. All these points suggest that probably there is one geothermal reservoir in the area, with spatial shape diversity.

Drilling and logging data, combined with the geochemical study in the cold groundwaters of the area, show that the main cold aquifers are not affected by the hot groundwaters (Kanellopoulos 2006, 2011; Kanellopoulos and Mitropoulos 2013). This implies that the hot reservoirs and the pathway of the hot groundwater are not in hydraulic connection with the main cold aquifers of the area.

The metamorphic rock formations, i.e. gneiss schists and greenstones, identified below Aedipsos and Ilia, are impermeable and work as a geothermal cap, having fault systems analysed above. Below these formations, carbonate rocks usually occur, within geothermal fluid circulation has been identified (Hatzis et al. 2008). In the Gialtra area, only thin layers (50, 180 m) of sediments were identified above the carbonate rocks. Perhaps the presence of the thick impermeable metamorphic rock formation is one of the reasons that the Aedipsos and Ilia hot springs present higher temperatures, and the springs are under pressure.

Also, in NW Euboea, almost all hot springs are actively depositing thermogenic travertine. Aedipsos is one of the largest active thermogenic travertine systems in Greece. They are composed mainly of calcite or aragonite or mixed calcite and aragonite as the main mineral phases (Kanellopoulos, 2011, 2012; Kanellopoulos et al. 2017a). After drying, travertine becomes very dense and impermeable,

although geothermal fluid circulation has been identified inside it. Most of the hot water boreholes are artesian; when near to clogging, they even create small geysers (some tens of centimetres high), indicative of the high pressure of the system. No sign of the three fault systems could be identified, due to the rapid deposition rate of the travertine. Most probably, the geothermal fluid reaches the surface of the bedrock and moves across the contact between bedrock and travertines. At the same time, because of the high pressure of the system, it uses fractures and moves upwards inside the travertine layer, creating several hot springs at the surface of the travertine cap. Daily changes in the water supply intensity of the hot springs were observed, which could be caused by geothermal pulses. These changes ought to be systematically measured and explained in the future.

Implications for geothermal exploration

The Northern Euboean Gulf and the neighbouring Sperchios Basin, on the mainland, occur in a unique back-arc geological position, at the western extremity of the North Anatolian Fault and in the vicinity of the Plio-Pleistocene Lichades volcanic centre, presenting one of the highest geothermal gradients in Greece. In NW Euboea, several hot springs occur, mainly in Aedipsos and two more in Gialtra and Ilia. Based on the information mentioned above, the groundwater flow pattern is primarily controlled by the tectonic setting of the area. The heat source is the magmatic chamber of the Lichades volcanic centre, at 7–8 km depth. Therefore, it could be concluded that the Euboea's hot springs occur as a result of both active tectonics of the area and recent volcanism and that below them there is one geothermal reservoir, with spatial shape diversity. Water recharge is achieved through the offshore faults, which are located at the seafloor of the Northern Euboean Gulf. These structures feed the system with seawater, which far below mixes with the deep geothermal fluid member, enriched in many conservative constituents and metals. During its upflow, the geothermal fluid does not show any indications of mixing with cold aquifers, although it reacts with the local geological formations. The Aedipsos hot springs have the minimum circulation depths, residence times and the most favourable tectonic setting (occurrence of three fault systems and with dense fault network), these data could explain the presence of so many hot springs, which present the maximum water discharge volume and temperature, compared to the other areas. Based on these, a conceptual flow pattern for the geothermal system can be delineated (Fig. 11).

The geothermal gradients were calculated for the three areas separately (Table 8) and show high thermal anomalies. The Gialtra area presents the lowest geothermal gradient, i.e. 7.8 °C/100 m, while at Ilia this is 10.4 °C/100 m. As far as Aedipsos is concerned, i.e. the area with the highest

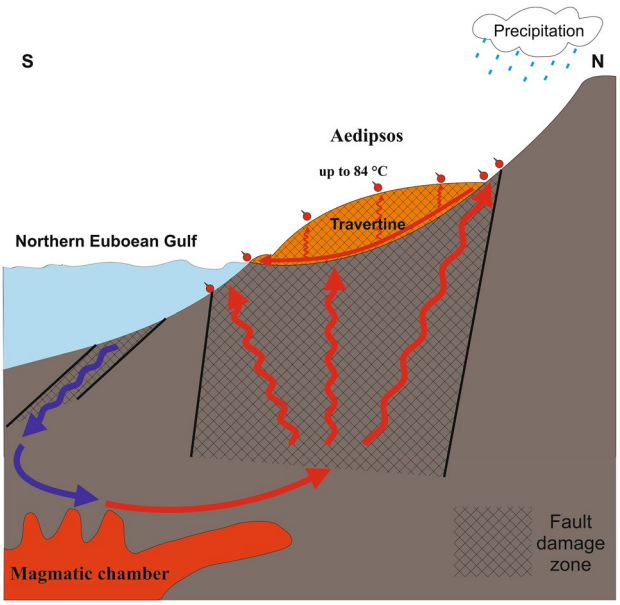

Fig. 11 Schematic hydrogeological flow pattern of geothermal fluids in the Aedipsos area, in Northwest Euboea

geothermal anomaly, two geothermal gradients were calculated. The first one is based on the AD-L-4 borehole (Hatzis et al. 2008) and amounts to 18.7 °C/100 m, which is considered as the most representative for the Aedipsos area. The second one is based on AD-G-20 borehole (Gkioni-Stavropoulou, 1998) and is 53.9 °C/100 m, which present the sharpest temperature increase with depth compared.

Until now, for the northwest of Euboea, the Greek State has recognized the area of Gialtra as a geothermal field available for economic exploitation (Government Gazette B′ 1058/2.6.2009). Based on the data of the Geothermal Energy Division, of the Greek Geological Survey (Hellenic Survey of Geology and Mineral Exploration-HGME, ex-IGME), NW Euboea has a potential geothermal heat capacity of about 26.4 MW_{th} (~ 4.4 MW_{th} in Gialtra; ~ 1 MW_{th} in Ilia and ~ 21 MW_{th} in Aedipsos, quantitative estimations).

Additionally, at the greater area, there are unexploited locations with high-chance to be hidden geothermal resources, such as areas NNE–SSW to NE–SW from Aedipsos; adding even more geothermal heat capacity.

In NW Euboea occurs a complex seawater-dominated, tectonically controlled and volcanic related geothermal systems, with active ore-mineralizing processes and serious potential geothermal heat capacity (~26.4 MW_{th}), which is waiting to be exploited properly, with respect to the history of the area and the already established installations for thermal spa/bathing therapies. A cascade utilization, i.e. combination of power production and direct-use applications such as heating of swimming pools, thermal baths (medical/wellness tourism), greenhouses, fish farming, etc., should be

considered in the frame of a sustainable development plan for the area.

Acknowledgements This study was funded by the National Strategic Reference Framework (NSRF, 350913). The authors would like to thank the local authorities, the local population and especially the Director of the Public Properties Company- Aedipsos branch, Ilia Siakantari for their co-operation during the fieldwork.

References

Anderberg MR (1973) Cluster Analysis for Applications. Academic Press, New York

Ambraseys N (2009) Earthquakes in the Mediterranean and Middle East: a multidisciplinary study of seismicity up to 1900. University Press, Cambridge **(ISBN 978 0 521 87292 8)**

Arnórsson S (2000) Isotopic and Chemical Techniques in Geothermal Exploration, Development and Use: Sampling Methods, Data Handling, Interpretation. International Atomic Energy Agency, Vienna, p 351

Athanasoulis K, Vakalopoulos K, Xenakis M, Persianis D, Taktikos S (2009) Periodical monitoring if hot springs of Greece. I.G.M.E, Athens **(in Greek)**

Athanasoulis K, Vougioukalakis G, Xenakis M, Kavouri K, Kanellopoulos C, Christopoulou M, Statha F, Rigopoulos P, Spagakos N, Tsigkas Th, Papadatou M (2016) Diachronic monitoring of hot springs and geothermal fields of Greece. I.G.M.E, Athens **(in Greek)**

Aubouin J (1959) Contribution a l'étude géologique 'de la Gréce septentrionale: les confins de l'Epire et de la Thessalie. Ann Géol Pays Hellen 10:1–483

Banks D, Odling NE, Skarphagen H, Rohr-Torp E (1996) Permeability and stress in crystalline rocks. Terra Nov. 8:223–235

Bebout GE, Ryan JG, Leeman WP (1993) B-Be systematics in subduction-related metamorphic rocks: characterization of the subducted component. Geochim Cosmochim Acta 57(10):2227–2237

Bellon H, Jarrige JJ, Sorel D (1979) Les activites magmatiques egeennes de l' Oligocene a nos jours et leurs cadres geodynamiques. Donnees nouvelles et synthese. Rev Géol Dynam Géog Phys 21:41–55

Caine JS, Evans JP, Forster CB (1996) Fault zone architecture and permeability structure. Geology 24:1025–1028

Charitakis K (1935) Healing springs and thermal bath cities of Greece. Anexartitos publ., Athens, p 16 **(in Greek)**

Cherdyntsev VV (1971) Uranium-234. Israel program for scientific translations, Jerusalem, p 234

Cherubini Y, Cacace M, Scheck-Wenderoth M, Moeck I, Lewerenz B (2013) Controls on the deep thermal field: implications from 3-D numerical simulations for the geothermal research site Groß Schönebeck. Environ Earth Sci Sp. https://doi.org/10.1007/s12665-013-2519-4

Cloutier V, Lefebvre R, Therrien R, Savard MM (2008) Multivariate statistical analysis of geochemical data as indicative of the hydrogeochemical evolution of groundwater in a sedimentary rock aquifer system. J Hydrol 353:294–313

Cumming W (2009) Geothermal resource conceptual models using surface exploration data. In: Proceedings 34th Workshop in Geothermal Reservoir Engineering, Stanford, 6 pp

Curewitz D, Karson J (1997) Structural settings of hydrothermal outflow: fracture permeability maintained by fault propagation and interaction. J Volcanol Geoth Res 79:149–168

D'Alessandro W, Brusca L, Martelli M, Rizzo A, Kyriakopoulos K (2010) Geochemical characterization of natural gas manifestations in Greece. Bull Geol Soc Greece 43(5):2327–2337

D'Alessandro W, Brusca L, Kyriakopoulos K, Bellomo S, Calabrese S (2014) A geochemical traverse along the "Sperchios Basin e Evoikos Gulf" graben (Central Greece): origin and evolution of the emitted fluids. Mar Pet Geol 55:295–308

D'Amore F, Fancelli R, Caboi R (1987) Observations on the application of chemical geothermometers to some hydrothermal systems in Sardinia. Geothermics 16:271–282

Damvergis A (1899) Hot waters in Aedipsos and the Thermae of Sylla. Blastos Publ., Athens, p 55 **(in Greek)**

Dotsika E (2015) H-O-C-S isotope and geochemical assessment of the geothermal area of Central Greece. J Geochem Explor 150:1–15. https://doi.org/10.1016/j.gexplo.2014.11.008

Fournier RO (1973) Silica in thermal waters: laboratory and field investigations. In: Proc. International Symposium on Hydrogeochemistry and Biogeochemistry, pp. 122–139 (Tokyo)

Fournier RO (1977) A review of chemical and isotopic geothermometers for the geothermal sys-tems. In: Proc. Symp. on geothermal energy, Cento Scient. Prog., Ankara, Turkey, 133-143

Fournier RO (1979) A revised equation for the Na-K geothermometer. Geotherm Res Council Trans. 3:221–224

Fournier RO, Potter RW (1979) Magnesium correction to the Na-K-Ca chemical geo-thermometer. Geochim Cosmochim Acta 43:1543–1550

Fournier RO, Truesdell AH (1973) An empirical Na-K-Ca geothermometer for natural waters. Geochim Cosmochim Acta 37:1255–1275

Fytikas M, Kolios N (1979) Preliminary heat flow map of Greece. In: Čermák V, Rybach L (eds) Terrestrial heat flow in Europe. Springer, Berlin, pp 197–205

Fytikas M, Giuliani O, Innocenti F, Marinelli G, Mazzuoli R (1976) Geochronological data on recent magmatism of the Aegean Sea. Tectonophysics 31:T29–T34

Fytikas M, Innocenti F, Manetti P, Mazzuoli R, Peccerillo A, Villari L (1985) Tertiary to Quaternary evolution of volcanism in the Aegean region, The Geological Evolution of the Eastern Mediterranean, Special Publ. Geol Soc 17:687–699

Galanakis D (1997) Neotectonic and stratihraphic of the neogene-quaternary sediments of Almyros-Pagasitikos, Pilio, Oreoi-Trikeri and Maliakos basins. Ph.D. Theses, University of Thessaloniki, Greece (**in Greek**)

Georgalas GC (1938) Le volcan des îles Likhades et de Hagios Ioannis (Kammena Vourla). Praktika Acad Athinion 13:86–98

Georgalas GC (1940) Über den chemismus der laven der vulkane von Lichadonissia, Wromolimni und Hagios Ioannis (Kamena Wourla). Praktika Acad Athinion 15:116

Geotermica Italiana (1984) Geotermica Italiana Methana – Poros – Loutraki – Sousaki -Platystomon - Aedipsos

Gidarikos D (1938) Geological and geomorphological study of the volcanic islands of Lichades and comparison with the Oeta Mountain and the coastline. Praktika Acad Athinion 13:99–107

Giggenbach WP (1981) Geothermal mineral equilibria. Geochim Cosmochim Acta 45:393–410

Giggenbach WF (1988) Geothermal solute equilibria: derivation of Na–K–Mg–Ca geoindicators. Geochim Cosmochim Acta 52:2749–2765

Giggenbach W, Sheppard D, Robinson B (1994) Geochemical structure and position of the Waiotapu geothermal field, New Zealand. Geothermics 23:599–644

Giggenbach WF, Stewart MK, Sano Y, Goguel RL, Lyon GL (1995) Isotope and geochemical techniques applied to geothermal investigations. IAEA-TECDOC 788:209–231

Gkioni-Stavropoulou G (1983) Inventory of hot and mineral springs of Greece, I, Aegean Sea. Hydrological and Hydrogeological Investigation Report No. 39, IGME, Athens (**in Greek**)

Gkioni-Stavropoulou G (1998) Hydrogeological study of hot and mineral springs of Euboean—Maliac gulf. IGME, Athens **(in Greek)**

Godinez MDC, Iturbe JL, Ordonez E, Solache-Rios M (1997) Determination of radium-226 in phosphate fertilizers and gypsum by gamma-ray spectrometry. Int J Environ Pollut 8:195–200

Goyal KP, Kassoy DFR (1980) Fault zone controlled charging of a liquid dominated geothermal reservour. J Geophys Resour 85(B4):1867–1875

Grant HLJ, Hannington MD, Hardardóttir V, Fuchs SH, Schumann D (2019) Trace metal distributions in sulfide scales of the seawater-dominated Reykjanes geothermal system: constraints on subseafloor hydrothermal mineralizing processes and metal fluxes. Ore Geol Rev. https://doi.org/10.1016/j.oregeorev.2019.103145

Hannington M, Garbe-Schönberg D (2019) Detection of gold nanoparticles in hydrothermal fluids. Econ Geol 114(2):397–400

Hannington M, Hardardóttir V, Garbe-Schönberg D, Brown KL (2016) Gold enrichment in active geothermal systems by accumulating colloidal suspensions. Nat Geosci. https://doi.org/10.1038/NGEO2661

Hardardóttir V, Hannington M, Hedenquist J (2013) Metal concentrations and metal deposition in deep geothermal wells at the Reykjanes high-temperature area, Iceland. Proc Earth Planet Sci 7:338–341

Hatzis M, Kavouridis Th, Bakalopoulos P, Xenakis M (2008) Investigation and determination of Northern Euboea geothermal fields. IGME, Athens **(in Greek)**

Henley RW, Truesdell A, Barton PBH Jr (1984) Fluid-mineral equilibrium in hydrothermal systems. In: Society of Economic Geologists, Reviews in Economic Geology, 1, p 267

Hernández-Antonio A, Mahlknecht J, Tamez-Meléndez C, Ramos-Leal J, Ramírez-Orozco A, Parra R, Ornelas-Soto N, Eastoe CJ (2015) Groundwater flow processes and mixing in active volcanic systems: the case of Guadalajara (Mexico). Hydrol Earth Syst Sci 19:3937–3950

Hochstein MP (1988) Assessment and modelling of geothermal reservoirs (small utilization schemes). Geothermics 17(1):15–49

Howarth R, Govett G (1983) Handbook of exploration geochemistry, vol. 2: statistics and data analysis in geochemical prospecting. Elsevier, Amsterdam

IAEA (2014) The Environmental Behaviour of Radium: Revised Edition. IAEA, technical reports series No. 476

IGME (1957) Geological map of Pelasgia in scale 1: 50,000, by Marinos, G., Anastopoulou, I., Maratou, G., Melidoni, N., Andronopoulou, V. I.G.M.E. Athens

IGME (1984) Geological map of Istiea in scale 1: 50,000, by Katsikatsos, G., Mettos, A., Vidakis, M. I.G.M.E. Athens

IGME (1991) Pagasitikos sheet, in scale 1: 200,000. Surficial sediment map of the Aegean Sea floor, by Perissoratis, C., Angelopoulos, I., Mitropoulos, D., Michailidis, S. I.G.M.E. Athens

Innocenti F, Agostini S, Doglioni C, Manetti P, Tonarini S (2010) Geodynamic evolution of the Aegean: constraints from the Plio-Pleistocene volcanism of the Volos-Evia area. J Geol SocLondon 167:475–489

Jolivet L, Faccenna C, Huet B, Labrousse L, Le Pourhiet L, Lacombe O, Lecomte E, Burov E, Denèle Y, Brun J-P, Philippon M et al (2013) Aegean tectonics: strain localisation, slab tearing and trench retreat. Tectonophysics 597–598:1–33

Kanellopoulos C (2006) Geochemical research on the distribution of metallic and other elements to the groundwater in Fthiotida Prefecture and N. Euboea. Master Thesis, University of Athens, Greece (in Greek)

Kanellopoulos C (2011) Geochemical research on the distribution of metallic and other elements in the cold and thermal groundwater, soils and plants in Fthiotida Prefecture and N. Euboea. Environmental impact. Ph.D. Thesis, University of Athens, Greece (in Greek with English abstract)

Kanellopoulos C (2012) Distribution, lithotypes and mineralogical study of newly formed thermogenic travertines in northern Euboea and eastern central Greece. Cent Eur Geosci 4(4):545–560

Kanellopoulos C (2013) Various morphological types of thermogenic travertines in northern Euboea and eastern central Greece. In: Bull. Geol. Soc. Greece, XLVII/3, pp 1929–1938

Kanellopoulos C (2014) Morphological types, lithotypes, mineralogy and possible bio-mineralization processes in simple and iron-rich travertines from active thermogenic travertine-forming systems in Greece. The cases of Northern Euboea and Eastern Central Greece. In: 19th International Sedimentological Congress-Abstracts book, p 341

Kanellopoulos C, Argyraki A (2013) Geochemical impact of hot springs and ultramafic rocks on soil, groundwater and vegetation: the case of NW Euboea, Greece. In: Chemie der Erde—Geochemistry, Vol. 73, Issue 4, p. 519-532

Kanellopoulos C, Mitropoulos P (2013) Geochemical effect of the rock chemistry and the anthropogenic activities on groundwater: the case of NW Euboea, Greece. In: Bull. Geol. Soc. Greece, vol. XLVII/2, p. 942-952

Kanellopoulos C, Lamprinou V, Mitropoulos P, Voudouris P (2015) Thermogenic travertine deposits in Thermopylae hot springs (Greece) in association with cyanobacterial microflora. Carbonates Evapor J. https://doi.org/10.1007/s13146-015-0255-4

Kanellopoulos C, Christopoulou M, Vakalopoulos P, Efthimiopoulos Xenakis THM (2016) Hydrochemical study of the hot groundwater of Ampelia area, Eastern Thessaly, Greece. A new area with geothermal interest. Greece. Bull Geol Soc Gr 5:710–719

Kanellopoulos C, Mitropoulos P, Valsami-Jones E, Voudouris P (2017a) A new terrestrial active mineralizing hydrothermal system associated with ore-bearing travertines in Greece (northern Euboea Island and Sperchios area). J Geochem Explor 179:9–24. https://doi.org/10.1016/j.gexplo.2017.05.003

Kanellopoulos C, Stouraiti C, Xenakis M, Vakalopoulos P, Vougioukalakis G (2017) The geothermal system of northwestern Euboea Island and eastern Sperchios areas, Greece: Geological characteristics and suggested direct use applications. In: 11th International Hydrogeological Congress of Greece, vol. 2, 263-273

Kanellopoulos C, Mitropoulos P, Argyraki A (2018a) Radiological and hydrochemical study of thermal and fresh groundwater samples of northern Euboea and Sperchios areas, Greece: insights into groundwater natural radioactivity and geology. Environ Monit Assess J 190:265. https://doi.org/10.1007/s10661-018-6643-1

Kanellopoulos C, Valsami-Jones E, Voudouris P, Stouraiti C, Moritz R, Mitropoulos P (2018b) A new occurrence of terrestrial native iron in the earth's surface: the Ilia thermogenic travertine case, northwestern Euboea, Greece. Geosci J 8:287. https://doi.org/10.3390/geosciences8080287

Kanellopoulos C, Thomas C, Xirokostas N, Ariztegui D (2019a) Banded Iron Travertines at the Ilia Hot Spring (Greece): an interplay of biotic and abiotic factors leading to a modern BIF analog? Deposit Rec. https://doi.org/10.1002/dep2.55

Kanellopoulos C, Vougioukalakis G, Mavrogonatos C, Megremi I, Iliopoulos I (2019b) Mineralogical, Petrological and Geochemical Study of the Agios Ioannis Volcanic Rocks, Kamena Vourla Area, Greece. Bull Geol Soc Gr 55:274–289. https://doi.org/10.12681/bgsg.21128

Karastathis V, Mouzakiotis E (2014) Combined onshore and offshore seismic investigations image fault structure at the geothermal field of Aedipsos-Yaltra, central Greece. EAG, First Break 32:61–65

Karastathis VK, Papoulia J, Di Fiore B, Makris J, Tsambas A, Stampolidis A, Papadopoulos GA (2011) Deep structure investigations of the geothermal field of the North Euboean Gulf, Greece, using 3-D local earthquake tomography and Curie Point Depth analysis. J Volcanol Geoth Res 206:106–120

Kati M, Voudouris P, Valsami-Jones E, Magganas A, Baltatzis E, Kanellopoulos C, Mavrogonatos K (2015) Cinnabar, arsenian pyrite and thallium-enrichment in active shallow submarine hydrothermal vents at Paleochori Bay, Milos Island, Greece. EGU 2015, Vienna, 17, EGU 2015-13046-2

Katsikatsos G, Mettos A, Vidakis M, Bavay P, Panagopoulos A, Basilaki A, Papazeti E (1982) Geological study of Aedipos area—Euboea. I.G.M.E. Geothemal studies (P.E.C.), Athens (in Greek)

Kelepertsis A, Tziritis E, Kelepertzis E, Leontakianakos G, Pallas K (2009) Hydrogeochemical characteristics and genetic implications of Edipsos thermal springs, north Euboea, Greece. Cent Eur J Geosci 1:241–250

Kharaka Y (1989) Chemical geothermometers and their application to formation waters from sedimentary basins. In: Naeser ND, McCulloh TH (eds) Thermal history of sedimentary basins. Springer-Verlag, New York, pp 99–117

Kilias SP, Nomikou P, Papanikolaou D, Polymenakou PN, Godelitsas A, Argyraki A, Carey S, Gamaletsos P, Mertzimekis TJ, Stathopoulou E, Goettlicher J, Steininger R, Betzelou K, Livanos I, Christakis C, Bell KC, Scoullos M (2013) New insights into hydrothermal vent processes in the unique shallow-submarine arc-volcano, Kolumbo (Santorini), Greece. Nat Sci Rep 3:2421

Kouskoukis K (2014) Healing tourism—Thermalism. Kafkas publ, Athens, p 290

Kranis H (1999) Neotectonic activity of Fault Zones in central-eastern mainland Greece (Lokris). Ph.D. Thesis, University of Athens, Greece (in Greek)

Lambrakis N, Kallergis G (2005) Contribution to the study of Greek thermal springs: hydrogeological and hydrochemical characteristics and origin of thermal waters. J Hydrogeol 13:506–521

Landerer X (1836) Description of Ypati, Aedipsos and Thermopylae hot springs. Royal Printing Office (**in Greek**)

Lindsey CR, Neupane G, Spycher N, Fairley JP, Dobson P, Wood T, McLing T, Conra M (2018) Cluster analysis as a tool for evaluating the exploration potential of Known Geothermal Resource Areas. Geothermics 72:358–370

Liu C-W, Lin K-H, Kuo Y-M (2003) Application of factor analysis in the assessment of groundwater quality in a blackfoot disease area in Taiwan. Sci Total Environ 313:77–89

Liu Y, Zhou X, Deng Z, Fang B, Tsutomu Y, Zhao J, Wang X (2015) Hydrochemical characteristics and genesis analysis of the Jifei hot spring in Yunnan, southwestern China. Geothermics 53:38–45

Lopez R, Garcia-Talavera M, Pardo R, Deban L, Nalda JC (2004) Natural radiation doses to the population in a granitic region in Spain. Radiat Prot Dos 111(1):83–88

Magri F, Akar T, Gemici U, Pekdeger A (2010) Deep geothermal groundwater flow in the Seferihisar-Balcova area, Turkey: results from transient numerical simulations of coupled fluid flow and heat transport processes. Geofluids 10:388–405

Margomenou-Leonidopoulou G (1976) Preliminary report of the research of Aidipsos thermometallic waters. In: Proc. of the International Congress on Thermal Waters. Geothermal Energy and Volcanism of the Mediterranean area, Athens, pp 340–351

Marini L, Fiebig J (2005) Fluid geochemistry of the magmatic-hydrothermal system of Nisyros (Greece). In: Hunziker, J.C., Marini, L. (Eds.), The Geology, Geochemistry and Evolution of Nisyros Volcano (Greece). Implications for the Volcanic Hazards. Memoires de Géologie (Lausanne), 44, 121–163

Marques JM, Carreira PM, Marques JE, Chaminé HI, Fonseca PE, Monteiro Santos FA, Eggenkamp HGM, Teixeira J (2011) The role of geosciences in the assessment of low-temperature geothermal resources (N-Portugal): a review. Geosci J 14:423–442

McGarth AG, Davison I (1995) Damage zone geometry around fault tips. J Struct Geol 17:1011–1024

McGuinness M, White S, Young R, Ishizaki H, Ikeuchi K, Yoshida Y (1995) A model of the Kakkonda geothermal reservoir. Geothermics 24:1–48

McKenzie D (1970) Plate tectonics of the Mediterranean Region. Nature 226:239–242

McKenzie D (1972) Active tectonics of the Alpide—Himalayan belt: the Aegean Sea and surrounding regions (Tectonics of the Aegean Region). Geophys J R Astron Soc. 55:217–254

Mitropoulos P, Kita I (1997) Geochemistry of oxygen and hydrogen isotopes in Greek regional waters. In: Proc 4th Hydrogeol. Congr., Hydrogeol. Commission of Greece

Mountrakis D (1986) The Pelagonian zone in Greece: A polyphase deformed fragment of the Cimmerian continent and its role in the geotectonic evolution of the Eastern

Nicholson K (1993) Geothermal fluids chemistry and exploration techniques. Springer-Verlag, Berlin

Ninkovich D, Hays JD (1972) Mediterranean island arcs and origin of high potash volcanoes. Earth Planet Sci Lett 16:331–345

Oliver MA (1990) Kriging: a method of interpolation for geographical information systems. Int J Geogr Inf Syst 4:313–332

Orfanos G (1985) Inventory of hot and mineral springs of Greece, Peloponnesus, Zakynthos, Kythira. Hydrological and Hydrogeological Investigation Report No. 39, IGME, Athens (in Greek)

Palmer CD, Ohly SR, Smith RW, Neupane G, McLing T, Mattson E (2014) Mineral selection for multicomponent equilibrium geothermometry. Transactions-Geothermal Resources Council 38

Pantosti D, De Martini PM, Papanastassiou D, Palyvos N, Lemeille F, Stavrakakis G (2001) A reappraisal of the 1894 Atalanti earthquake surface ruptures, central Greece. Bull Seismol Soc Am 91(4):760–780

Palyvos N (2001) Geomorphological study of the broader Atalanti area. Ph.D. Thesis, National and Kapodistrian University of Athens, p 234 (**in Greek**)

Papanikolaou D (1939) Aedipsos. Thermal water bath therapy, Mud bath therapy, Climate therapy. Their effect on healing long lasting diseases. Ph.D., Athens University, p 67 (**in Greek**)

Parks MM, Caliro S, Chiodini G, Pyle DM, Mather TA, Berlo K, Edmonds M, Biggs J, Nomikou P, Raptakis C (2013) Distinguishing contributions to diffuse CO_2 emissions in volcanic areas from magmatic degassing and thermal decarbonation using soil gas 222Rn and 13C systematics: application to Santorini volcano, Greece. Earth Planet Sci Lett 377–378:180–190

Pe G (1975) Strontium isotope ratios in volcanic rocks from the northwestern part of the Hellenic arc. Chem Geol 15(1):53–60

Pe G, Panagos A (1976) Comparative geochemistry of the Northern Eubeoecos 26 lavas. Bull Geol Soc Greece 9:95–133 **(in Greek)**

Pe-Piper G, Piper D (1989) Spatial and temporal variation in Late Cenozoic back-arc volcanic rocks, Aegean Sea region. Tectonophysics 169(1–3):113–134

Pe-Piper G, Piper D (2002) The igneous rocks of Greece, the anatomy of an orogeny. Ge-bruder Borntraeger, Berlin

Pe-Piper G, Piper DJW (2007) Neogene back-arc volcanism of the Aegean. new insights into the relationship between magmatism and tectonics. Geol Soc Am Spec Pap 418:17–31

Pertessis M (1937) Thermomineral Springs of Greece. Institute of Geology and Mineral Exploration, Report No. 24. Athens (in Greek)

Price RE, Savov I, Planer-Friedrich B, Bühring SI, Amend J, Pichler T (2013) Processes influencing extreme As enrichment in shallow-sea hydrothermal fluids of Milos Island, Greece. Chem Geol 348:15–26

Ring U, Glodny J, Will Th, Thomson S (2010) The Hellenic Subduction System: high-Pressure Metamorphism, Exhumation, Normal Faulting, and Large-Scale Extension. Annu Rev Earth Planet Sci 38:45–76

Roberts S, Jackson J (1991) Active normal faulting in central Greece: an overview. Geol Soc Lond Sp Publ 56(1):125–142

Sakellariou D, Rousakis G, Kaberi H, Kapsimalis V, Georgiou P, Kanellopoulos Th, Lykousis V (2007) Tectono-sedimentary structure and Late Quaternary evolution of the North Evia Gulf basin, central Greece: preliminary results. Bull Geol Soc Greece 40:451–462

Scherreiks R (2000) Platform margin and oceanic sedimentation in a divergent and convergent plate setting (Jurassic, Pelagonian Zone, NE Evvoia, Greece). Int J Earth Sci 89:90–107

Sfetsos KS (1988) Inventory of hot and mineral springs of Greece, III, Mainland Greece. Hydrological and Hydrogeological Investigation Report No. 39, IGME, Athens (in Greek)

Shaw B, Jackson J (2010) Earthquake mechanisms and active tectonics of the Hellenic subduction zone. Geophys J Int 181:966–984

Shimizu A, Sumino H, Nagao K, Notsu K, Mitropoulos P (2005) Variation in noble gas isotopic composition of gas samples from the Aegean arc, Greece. J Volcanol Geotherm Res 140(4):321–339

Spycher N, Peiffer L, Sonnenthal EL, Saldi G, Reed MH, Kennedy BM (2014) Integrated multicomponent solute geothermometry. Geothermics 51:113–123

Stober I, Bucher K (2002) Water-rock interaction. Springer-Science and Business Media, B.V

Tassi F, Capecchiacci L, Gianninia GE Vougioukalakis, Vaselli O (2013a) Volatile organic compounds (VOCs) in air from Nisyros Island (Dodecanese Archipelago, Greece): natural versus anthropogenic sources. Environ Pollut 180:111–121

Tassi F, Vaselli O, Papazachos CB, Giannini L, Chiodini G, Vougioukalakis GE, Karagianni E, Vamvakaris D, Panagiotopoulos D (2013b) Geochemical and isotopic changes in the fumarolic and submerged gas discharges during the 2011–2012 unrest at Santorini caldera (Greece). Bull Volcanol 75:711–726

Truesdell AH (1976) Summary of section III—geochemical techniques in exploration. In: Proceedings of the 2nd U.N. Symposium on the Development and Use of Geothermal Resources, San Francisco, 1, liii-lxxix

Truesdell AH, Thompson JM, Coplen TB, Nehring NL, Janick CJ (1981) The origin of the Cerro Prieto geothermal brine. Geothermics 10(3/4):225–238

Tzitziras A, Ilias P (1996) Geotechnical study of Loutra Edipsou peripheral road. IGME, Athens **(in Greek)**

Vakalopoulos P, Metaxas A, Xenakis M (2000) Research and evaluation of lignite resources in Euboea Island: Northern Euboea basin. Report of IGME, p 35 (**in Greek**)

Valsami-Jones E, Baltatzis E, Bailey EH, Boyce AJ, Alexander JL, Magganas A, Anderson L, Waldron S, Ragnarsdottir KV (2005) The geochemistry of fluids from an active shallow submarine hydrothermal system: milos island, Hellenic Volcanic Arc. J Volcan Geother Res 148:130–151

Vavassis I (2001) Geology of the Pelagonian zone in Northern Evia Island (Greece): Implications for the geodynamic evolution of the Hellenides. These de doctorat, Univ. de Lausanne, Switzerland

Vega M, Pardo R, Barrado E, Deban L (1998) Assessment of seasonal and polluting effects on the quality of river water by exploratory data analysis. Water Res 32:3581–3592

Vött A (2007) Relative sea level changes and regional tectonic evolution of seven coastal areas in NW Greece since the mid-Holocene. Quatern Sci Rev 26(7–8):894–919

Voudouris KS, Lambrakis NJ, Papatheothorou G, Daskalaki P (1997) An application of factor analysis for the study of the hydrogeological conditions in Plio-Pleistocene aquifers of NW Achaia (NW peloponnesus, Greece). Math Geol 29:43–59. https://doi.org/10.1007/BF02769619

Voutetakis S, Fytikas M (1975) Study for the geothermal energy in Greece. Report No 54, I.G.M.E. Athens (in Greek)

Voutsis N, Kelepertzis E, Tziritis E, Kelepertsis A (2015) Assessing the hydrogeochemistry of groundwaters in ophiolite areas of Euboea Island, Greece, using multivariate statistical methods. J Geochem Explor 159:79–92

Wang J, Jin M, Jia B, Kang F (2015) Hydrochemical characteristics and geothermometry applications of thermal groundwater in northern Jinan, Shandong, China. Geothermics 57:185–195

Yoshida Y, Nakazawa T, Yoshikawa H, Nakanishi T (2009) Partition coefficient of Ra in gypsum. J Radioanal Nucl Chem 280:541–545

Zhou Q, Birkholzer JT, Tsang CF, Rutqvist J (2008) A method for quick assessment of CO_2 storage capacity in closed and semi-closed saline formations. Int J Greenh Gas Control 2(4):626–639